Structural control of dykes and veins in the Mansikka-aho area, Evijärvi, Western Finland

Teo Lehto

Master's thesis

University of Turku
Department of Geography and Geology
Geology section

June 2021

UNIVERSITY OF TURKU
Department of Geography and Geology, Geology section
LEHTO, TEO: Structural control of dykes and veins in the Mansikka-aho area, Evijärvi, Western Finland
MSc thesis, 52 pages + 4 appendix pages
Geology and mineralogy
June 2021
The originality of this thesis has been checked in accordance with the University of Turku quality assurance system using the Turnitin OriginalityCheck service.

The northern part of the Aho metavolcanic belt within Ostrobothnia schist belt has been explored intensively because of the vicinity of the discovered spodumene pegmatite deposits in the Kaustinen area. The aim of this study is to carry out a model of the structural geometry and evolution of the bedrock in the southern part of the Aho belt (Mansikka-aho, Evijärvi) and to study the structural control of pegmatite dykes and quartz veins in the study area. The study area was mapped, and oriented handheld drill core samples were acquired during the field seasons of 2019 and 2020. Thin sections were made from the oriented core samples. Petrographic analysis of the lithologies and a structural analysis were carried out based on the bedrock observations and the oriented thin sections.

The bedrock of the study area is composed of mica schists, black schists, metavolcanic rocks, felsic intrusions, quartz veins and pegmatite and aplite dykes. Primary structures are preserved throughout the study area. Three types of foliations are present: (1.) the NE-SW-trending foliation which is commonly the most significant structural feature at the central and western parts of the study area, (2.) weak NW-SE foliation at the northern parts of the study area and (3.) a foliation parallel to the S0. The quartz veins and pegmatite dykes are often planar and cut the structures of the host rock, but it is common that the veins and dykes are parallel or sub parallel to the trend of the foliation or the primary bedding.

The study area is characterized by a plunging synform and an overturned plunging antiform with fold axes pointing towards SW. This structure is a part of the regional open fold within Ostrobothnia schist belt. The stratigraphy of the study area is overturned from its original depositional position. The geometry of the study area is controlled by NE-trending shear zones located north and south of the study area. The study area represents a shear-bound block which got its final geometry because of a transpressional clockwise rotation between the shear zones. At least three major deformation events have occurred within the study area: D1 which is related to regional-scale thrusting systems and isoclinal folding, D2 which represents the peak of the deformation and the most dominant structural features and D3, which can be seen as crenulation cleavage S3. The metamorphism in the study area occurred at medium pressure and high temperature conditions. The intrusion of the pegmatite veins and the quartz veins in the supracrustal rocks are controlled by the structures of the bedrock, but also by the lithology. The veins and dykes are emplaced at the older planar structures such as the foliation and the bedding planes. The psammite interlayers in supracrustal rocks host most of the quartz veins while they are less common in pelitic layers.

Keywords: structural geology, pegmatites, dykes, lithium

TURUN YLIOPISTO
Maantieteen ja geologian laitos, geologian osasto
LEHTO, TEO: Structural control of dykes and veins in the Mansikka-aho area, Evijärvi, Western Finland
Pro gradu -tutkielma, 52 sivua + 4 liitesivua
Geologia ja mineralogia
Kesäkuu 2021
Turun yliopiston laatujärjestelmän mukaisesti tämän julkaisun alkuperäisyys on tarkastettu Turnitin Originality Check -järjestelmällä.

Pohjanmaan liuskevyöhykkeellä sijaitsevan Ahon metavulkaniittijakson pohjoisosaa on tutkittu aktiivisesti Kaustisen alueella sijaitsevien spodumeenipegmatiittiesiintymien takia. Tämän tutkimuksen tavoitteena on luoda malli Ahon jakson eteläosan (Mansikka-aho, Evijärvi) kallioperän rakenteellisesta geometriasta ja kehityksestä ja tutkia tätä mallia hyödyntäen tutkimusalueen pegmatiitti- ja kvartsijuonten paikalleen asettumista kontrolloivia tekijöitä. Tutkimusalue kartoitettiin ja alueen kallioperästä otettiin suunnattuja minikairanäytteitä kenttäkesien 2019 ja 2020 aikana. Näytteistä tehtiin suunnattuja ohuthieitä. Havainto- ja ohuthieaineiston pohjalta alueen kallioperästä tehtiin petrografinen ja rakenteellinen analyysi.

Tutkimusalueen kallioperän muodostavat kiilleliuske, mustaliuske, metavulkaniitit, felsiset intruusiot sekä kvartsi-, pegmatiitti- ja apliittijuonet. Primäärejä kallioperän rakenteita on erotettavissa lähes koko tutkimusalueella. Tutkimusalueen liuskeisuudet ovat jaettu kolmeen tyyppiin: (1.) koillinen-lounas-suuntainen liuskeisuus, joka on tyypillisesti paljastumien voimakkain rakenne-elementti, (2.) heikko luode-kaakko-suuntainen liuskeisuus tutkimusalueen pohjoisosassa ja (3.) kerroksellisuuden suuntainen liuskeisuus. Kvartsi- ja pegmatiittijuonet ovat tavallisesti tasomaisia ja isäntäkivien rakenteisiin nähden leikkaavia, mutta yleisesti juonet ovat samansuuntaisia liuskeisuuden tai kerroksellisuuden kanssa.

Tutkimusalueen alueen yleistä rakennegeometriaa luonnehtivat akseliltaan lounaaseen kaatuva synformi ja ylikaatunut antiformi. Nämä poimurakenteet ovat osa laajempaa avointa alueellista poimua Pohjanmaan liuskevyöhykkeellä. Tutkimusalueen alueen stratigrafia on ylikaatunut alkuperäiseltä kerrostumisjärjestykseltään. Tutkimusalueen tämänhetkistä rakennegeometriaa ovat kontrolloineet tutkimusalueen pohjois- ja eteläpuolella sijaitsevat koillisen suuntaiset hiertovyöhykkeet, ja niiden välissä myötäpäivään tapahtunut transpressionaalinen rotaatio. Tutkimusalue on käynyt läpi ainakin kolme eri deformaatiovaihetta: D1, johon liittyvät alueellismittakaavainen ylityöntö ja isokliininen poimutus, D2, joka edustaa deformaation huippua ja tutkimusalueen voimakkaimpia deformaatiorakenteita, ja D3, joka on aiheuttanut S2:n krenulaatioliuskeisuuden. Tutkimusalueen metamorfoosin huippu on tapahtunut keskitasoisessa paineessa ja korkeassa lämpötilassa. Litologia ja aiemmat tasorakenteet, kuten liuskeisuus- ja kerroksellisuustasot, ovat kontrolloineet kvartsi- ja pegmatiittijuonten paikalleenasettumista. Juonet ovat tyypillisesti suprakrustisten kivien psammiittisissa kerroksissa, kun taas juonten esiintyminen peliittisissä kerroksissa on harvinaisempaa.

Avainsanat: rakennegeologia, pegmatiitit, juonet, litium

Table of Contents

1. Introduction

According to OECD, the demand of raw materials is going to double by 2060 (Blengini et al., 2020). This increase is due to growing global population, digitalization, industrialization and transition from fossil fuel dependence to climate neutrality. The increase in demand comes largely from the developing countries. Sustainable technologies and products demand large amounts of raw materials, and based on their economic importance and supply risk, the European Union has created a list of Critical Raw Materials. About 80 % of raw materials are imported to European Union. The production of the raw materials is concentrated on countries outside EU and especially the role of China as leading exporter has raised concern. For example, China supplies 98 % of the rare earth elements imported to EU. The Critical Raw Materials list was updated in 2020 and it contains 30 raw materials that are crucial to strategically essential sectors of renewable energy, electric cars, digital infrastructure and space and defence technology.(Blengini et al., 2020)

Geological Survey of Finland (GTK) launched a four-year project (2019-2022) focusing on evaluating the mineral potential of battery elements and minerals in Finland. The most important of these elements are lithium, cobalt and graphite, which are all included in the new EU Critical Raw Materials list. 87 % of the EU sourcing extraction-stage lithium is imported from Australia and 78 % of processing-stage lithium is supplied from Chile. 68 % of the EU sourcing extraction stage cobalt comes from the Democratic Republic of the Kongo and 47 % of natural graphite comes from China (Blengini et al., 2020). The aim of the GTK's project is to recognize new areas where discovering new potential battery mineral deposits is possible. The emphasis of this new project in Central and Southern Ostrobothnia is to evaluate the mineral potential of lithium and cobalt.

In Finland, cobalt, nickel, graphite and lithium are among the elements which are crucial to the battery industry and are abundant in the Fennoscandian bedrock. Interest towards the study and exploration of pegmatites have been significant as the known lithium deposits and undiscovered resources in Finland occur in LCT (lithium-cesium-tantalum) type pegmatites. The Geological Survey of Finland estimated lithium resources of Finland from the undiscovered LCT-pegmatite deposits, and they concluded that over 90 % of the undiscovered lithium resources in Finland can be found in Kaustinen or the surrounding

Järvi-Pohjanmaa area (Rasilainen et al., 2018). Six well known LCT pegmatite deposits are known from the Kaustinen area but over 90 % of the undiscovered lithium resources in Finland are expected to be in unknown or weakly studied areas. Evijärvi and the area of interest of this study is located in the vicinity of the spodumene pegmatites of Kaustinen, where mining and chemical company Keliber is planning to initiate lithium hydroxide production from spodumene ore (Rasilainen et al., 2018).

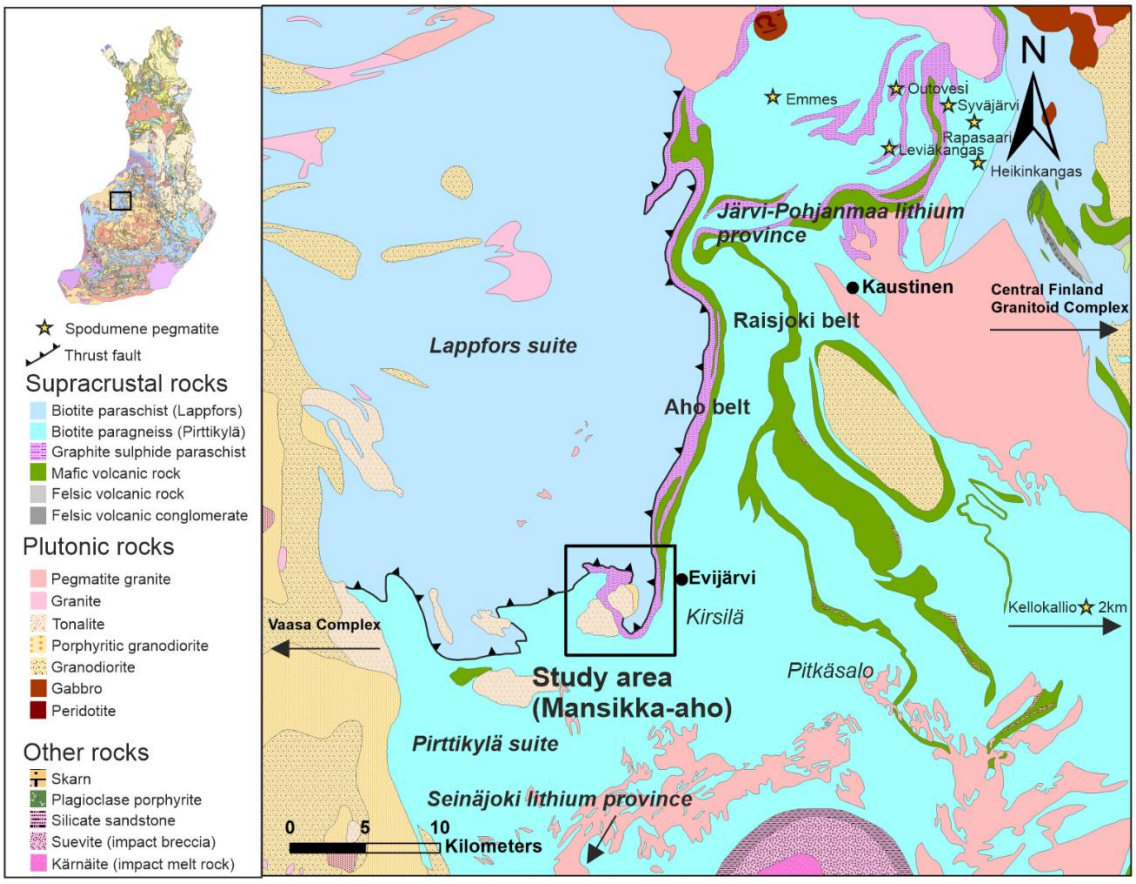

Figure 1. Bedrock map of the study area and the surrounding Ostrobothnia Schist Belt. Bedrock map modified after Geological Survey of Finland.

The structural control of pegmatites is not as studied subject as petrography, mineralogy and geochemistry of pegmatites. It is expected that pegmatites prefer competent lithologies and structural weakness zones such as lithological contacts, bedding and foliation planes and faults (Dill, 2015). For example, in one of the largest lithium pegmatite deposits in the world, Greenbushes, Australia, the pegmatites are placed along the Archean crustal scale shear zone (Partington, 1990). In Monts d'Ambazac, France, and Pedra Lavrada, Brazil, the pegmatites and faults have a distinct relationship (Deveaud et al., 2013; Sales et al., 2016). 50 % of the studied pegmatites in Monts d'Ambazac are

located less than 500 meters away from the studied faults and the pegmatite clusters tend to have a parallel orientation with a large-scale shear zone and the associated faults. The fault patterns and pegmatites were linked and had the same orientation also in Pevra Lavrada, Brazil. The reactivation of weakness planes, such as bedding and fault planes, was the initial process for pegmatite placement in Rwamagana-Musha-Ntunga area, Rwanda (Hulsbosch et al., 2017). This reactivation was controlled by the lithology and competence difference in host rocks.

According to Ahtola et al., (2015), 16 spodumene pegmatite deposits are known in Ostrobothnia. The spodumene pegmatites are typically placed relatively close to larger pegmatite granite intrusions and occurring along the contacts of mica schists and intermediate metavolcanic rocks. The pegmatites have varying widths from 1 to 25 meters and their length reach up to 700 meters. Many of the pegmatites, such as Leviäkangas, Syväjärvi, Rapasaari and Kellokallio in Central Ostrobothnia (Fig. 1), have strike approximately to N-S or NW-SE. The emplacement of the spodumene pegmatites of Rapasaari, Syväjärvi and Kellokallio are interpreted to be controlled by structures related to a fold, but detailed structural study has not been made within these deposits. (Ahtola et al., 2010; Kuusela et al., 2011; Kuusela & Kaunismäki, 2020). The study area is located between the lithium provinces of Seinäjoki and Järvi-Pohjanmaa. Potential for cobalt has earlier been recognized from the sulphide and black schists of the Raisjoki metavolcanic belt (Ruskeeniemi, 1988).

The aim of this study was to understand the potential structural and lithological control of the pegmatite dykes within the *Mansikka-aho* area, Evijärvi (*Fig. 1*). Since no systematic structural analysis had been conducted in the area, this work also aimed at providing a structural framework for the area. The study of the structural control of the pegmatites can be utilized in pegmatite exploration and in modelling the continuity of the known pegmatite deposits.

In order to study the structure of the hosting rocks and the structural control of the pegmatites, the study area was mapped, and oriented handheld drill core samples were acquired during the field seasons of 2019 and 2020 (*Fig. 2*). Thin sections were made from the oriented core samples. The petrographic analysis of the lithologies and the structural analysis were carried out based on the field observations and the oriented thin sections. The structural analysis involved assessment of the structural geometry,

kinematics and the relative age relationships of the lithologies and the structures. Moreover, the structural data was used to create a paleo stress field model on the intrusion of the pegmatites. As the pegmatite data from the study area is somewhat limited quartz vein observations are used in supplementing the data needed for stress field modelling.

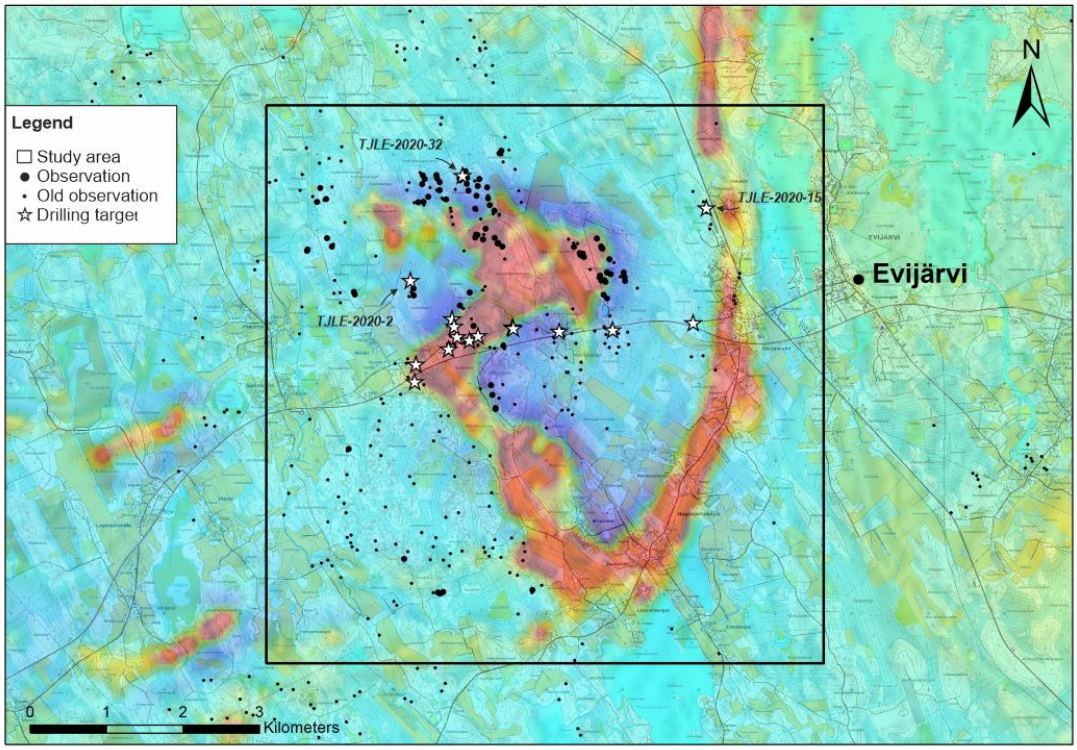

Figure 2. Aeromagnetic map of the study area with locations of the bedrock observations and the drilling targets. E-W profile through the lithologies were drilled in 2019. Three locations (TJLE-2020-2, TJLE-2020-15 and TJLE-2020-32) were drilled in 2020. Aeromagnetic map modified after the Geological Survey of Finland.

This thesis presents a model of the structural evolution of the study area. The model includes a description about the structural geometry of the study area and the systematics of the occurrence of the pegmatite dykes and quartz veins in the study area. The main results of this study indicate that the position of the dykes and veins are controlled by both the preceding structures and the lithology and the local and regional stress fields. The emplacement of the dykes and veins within the supracrustal rocks occurred in a stress field with sigma 3 in N-S direction and are related to the opening of the primary bedding and secondary foliation planes. By contrast, the dykes and veins at the plutonic intrusions parallel and perpendicular to the contact of the intrusion are more likely related to the brittle structures formed in a local stress field as the intrusions contracted during cooling of the intrusive body.

2. Geological setting

The study area is located within Evijärvi municipality, Southern Ostrobothnia. This area is part of the Ostrobothnian Paleoproterozoic Svecofennian schist belt (Simonen, 1980). Central Finland Granitoid Complex is situated east from the schist belt. The Ostrobothnia schist belt is dominated by turbiditic metagreywackes and metapelites. Felsic intrusions, metavolcanic belts and black schists also occur among the typical supracrustal rocks (Vaarma & Pipping, 1997). The two N-S oriented metavolcanic belts of Aho and Raisjoki (*Fig. 1*) are geochemically mafic to intermediary. These metavolcanic rocks are typically massive and homogeneous. The grain size of the metavolcanic rocks varies from fine to medium grained and some parts of the metavolcanics belts show oriented textures. Thin mafic and intermediate tuffite layers, as well as carbonate and black schists layers occur in the Aho belt (Vaarma & Kähkönen, 1994). According to the old observation data from the GTK database, some outcrops belonging to the Aho metavolcanic belt can be found in the northeastern corner of the study area. The volcanic rocks are mafic, rich in hornblende and have pillow lava-type texture meaning that these rocks might be related to pillow lavas near the Aho village 5 kilometers north from the study area. The rocks are homogeneous and fine grained but have occasionally coarser parts. The metavolcanic rocks in the study area are characterized by a large number of joints and cavities caused by weathering of softer material such as carbonate minerals. Carbonates occur also as dykes in the metavolcanic rock. Tuffite layers can be seen among the volcanic rock. Black schist layers are usually sulphide schists or sulphide-graphite schists and they have a composition related to a pelitic origin (Marmo, 1960). The study area is mainly composed of black schists and sulphide metagreywackes. Two tonalite intrusions in the study area are light-coloured, even-grained, massive and coarse-grained (Vaarma & Pipping, 1997). Greywacke xenoliths are common in both intrusions. Generally, the xenoliths are small, angular, dark and fine grained.

The grade of metamorphism in Ostrobothnia belt rises from east to west/southwest. Multiple generations of deformation are known from the Southern Ostrobothnia, and the peak of deformation and the peak of regional amphibolite facies metamorphism are the same age. These events occurred earlier than the emplacement of the tonalite intrusions (1883 ± 6 Ma), which does not display signs of deformation. (Vaarma & Pipping, 1997).

A thrust fault between the sulphide graphite schist and Lappfors suite metagreywacke and between the metagreywacke and the Pirttikylä suite mica gneiss is presented in the bedrock map (*Fig. 1*; Geological Survey of Finland, 2021). The main trend of the magnetic and electromagnetic form lines outside the study area is roughly NE-SW.

3. Materials & methods

3.1. Bedrock observations

Bedrock observations from 116 localities within the Mansikka-aho area were made during the summer field seasons of 2019 and 2020. The observations were collected with Android-based mobile application Kapalo provided by GTK. The observation data included for example GPS-location, rock type, grain size, colour, planar and linear structures, field photo and minerals. 77 of the observations contain measurements of structural elements made with a geological compass. 36 field sketches were drawn from the observation points. The study area contains 272 old bedrock observations acquired from the GTK database. These old observations include 138 structural measurements.

In general, the bedrock outcrops in the study area are scarce and small. The tonalite and the granodiorite intrusions are exposed well. The intrusions host four construction aggregate quarries which are key outcrops in the area. The sulphide graphite schist is exposed poorly, and it is challenging to observe structures from these rocks. The metagreywacke and mica schist are generally poorly exposed but in some places outcrops can be found fairly well. These outcrop clusters occur for example in Kalliokangas, Varsakalliot and in Hyytiäisahonkangas (*Fig. 3*).

3.2. Thin sections

In total, 38 oriented samples from 16 observation locations were collected by a handheld rock drill. 26 of these samples were taken as a profile through all the lithologies in the study area during the summer of 2019. These lithology samples were taken from 13 locations, with 2 samples taken from each location. 12 samples were collected during the

summer of 2020. These samples were drilled from 3 locations with porphyroblast-bearing metasediments to study the age relationship of the porphyroblast growth and the foliation. 24 oriented thin sections were prepared from the samples by Arto Peltola at the Geohouse, Turku. The thin sections were used to study the petrography and the microstructures of the rocks in the study area.

3.3. Geophysical and bedrock maps

Geophysical maps and bedrock maps were used during bedrock mapping, sampling and structural analysis. Processed aerogeophysical magnetic and electromagnetic maps were used before fieldwork when interpreting structural form lines from the study area (Geological Survey of Finland, 2021). The flight lines in Evijärvi area are from east to west and the line spacing is 200 meters. The graphite sulphide schists produce the high total intensity magnetic anomaly in the study area. 1:10 000 basic map raster was used as a base map within the Kapalo software (National Land Survey of Finland, 2021). The scale free bedrock map was used throughout the study (Geological Survey of Finland, 2021). This bedrock map is vector-based and has 1:200 000 scale in Evijärvi area. In addition to the rock type polygons, the scale free bedrock map includes interpreted faults, magnetic and electromagnetic form lines and dykes.

4. Results

4.1. Lithology of the study area

The dominant supracrustal rock unit in the study area is Svecofennian mica schist with graphite and sulphide rich interlayers. The Aho metavolcanic and graphite sulphide belt cuts the study area (*Fig. 1*). The N-S metavolcanic sequence runs through the northeastern part of the study area until it bends west and north and furthermore west at the central part of the study area. The metavolcanic rock is exposed only in the northeastern part of the study area and the sequence which generates the magnetic anomaly in the study area seems to be dominantly graphite sulphide schist. Two plutonic intrusions are placed along

the supracrustal rocks. Granite, aplite and pegmatite dykes are common in all of the lithological units in the study area.

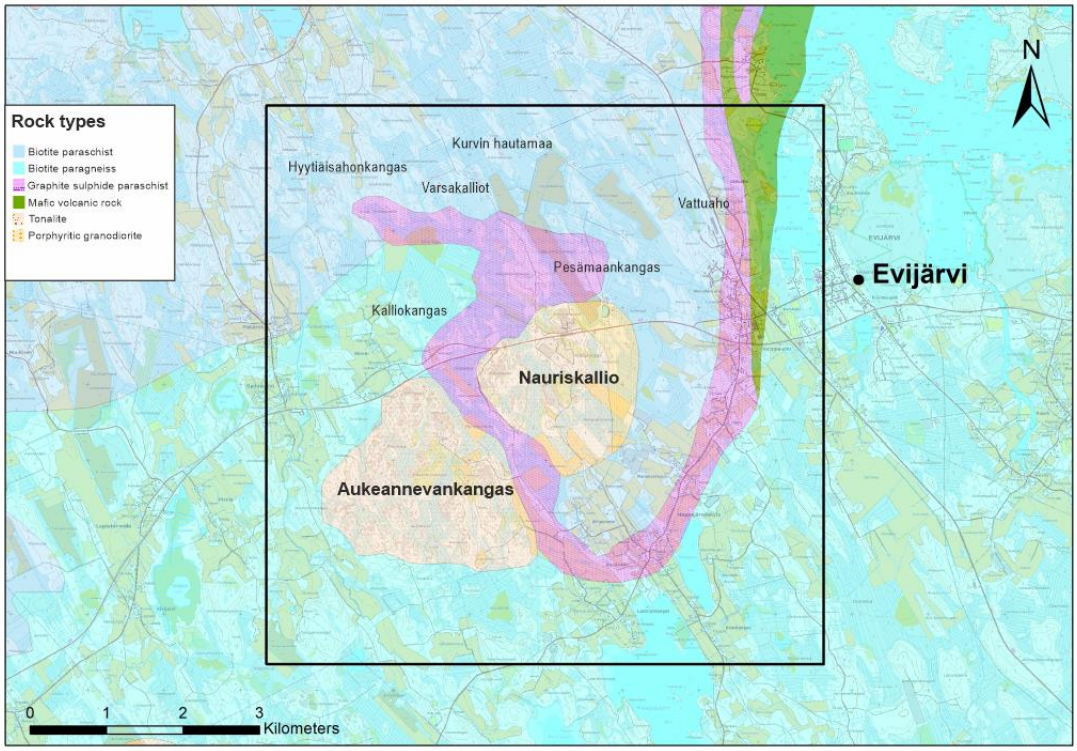

Figure 3. Generalised bedrock map of the study area. Bedrock map from Geological Survey of Finland. Base map from National Land Survey of Finland.

4.1.1. Supracrustal rocks

The supracrustal sedimentary rocks in the study area have layering which varies from pelitic to psammitic in composition. The layer thickness ranges from 10 cm to 1-2 meters (*Fig. 4a*). The color of the sedimentary rocks is medium grey, but the pelite rich layers have a slightly darker shade than the psammitic layers (*Fig. 4b, 4c*). The biotite, muscovite, quartz and feldspar matrix of the sedimentary rocks is fine grained but 1 – 10 mm porphyroblasts are common. Primary textural features such as graded bedding and load casts are commonly visible. Porphyroblasts are common especially in the layers with pelitic origin. At the psammitic layers, the porphyroblasts are less common and their grain size is smaller. Four types of porphyroblasts are present in the mica schists. The largest and macroscopically easily visible porphyroblasts are usually fibrous sillimanite

(fibrolite) or andalusite. These brown fibrolite porphyroblasts does not have inclusions and occasionally they are elongated in the direction of the schistosity.

Figure 4. Characteristic supracrustal rocks of the study area. A) Calc-silicate concretions in a layered mica schist. The foliation bottom left to top right in image is perpendicular to the bedding. TJLE-2020-32. B) Bedding (S0) in metagreywacke. TJLE-2020-2. C) Primary bedding in mica schist. TJLE-2020-15. D + E) Weathering surface of the graphide sulphide mica schist. D: TJLE-2019-9, E: TJLE-2019-11. Rock hammer head and pen pointing north.

Approximately 25 x 20 cm calc silicate concretions can be seen throughout the supracrustal rocks in the study area. Concretions can act as indicators of the strain, as the elongated calc-silicate concretion in *figure 7b*. Quartz veins in supracrustal rocks are typically 0,3 to 1 cm thick and they are more abundant within the psammite rich layers.

The graphite and sulphide bearing interlayers occur in the sedimentary sequence (*Fig. 4d*). Usually, the layers are thin and the amount of sulphides is low but occasionally the graphite and sulphide content is fair or high (Fig. 4e). The black schist layers are non-magnetic to very weakly magnetic. The structures and textures cannot be identified because the appearance of the black schist outcrops is rusty brown and highly weathered.

4.1.2. Plutonic rocks

The western intrusion in the study area is called Aukeannevankangas and the eastern intrusion is Nauriskallio (*Fig. 3*). The intrusions are homogeneous and medium grained (2-5 mm) tonalite (*Fig. 5a*). Usually, the colour of the tonalite is grey to light grey but sometimes reddish as the K-feldspar content rises (*Fig. 5b*). Approximately 50 – 60 % of the minerals are feldspar, 15 – 25 % quartz and 20 – 25 % biotite. The occurrence of the reddish K-feldspar varies in different areas of the intrusions from 0 % to 50 % (*Fig. 5c, 5d*). The intrusions occasionally display an elongation parallel to the orientation of the mica grains. Sometimes the fragments are granitic or granodioritic in composition and their size vary from few centimeters up to half meters. Porphyritic granodiorite can be found in S and SE parts of the Aukeannevankangas (*Fig. 3*) intrusion and NW part of the Nauriskallio. The porphyres in Aukeannevankangas are pinkish feldspar from 2 to 5 millimeters in diameter. In SE part the porphyres are plagioclase and have greenish tint and pyrite and pyrrhotite are also present. In Nauriskallio, the light grey feldspar porphyres are 1 – 3 cm and many porphyres have a quartz core. The grain size of the matrix in the porphyritic granodiorite is approximately 1 mm.

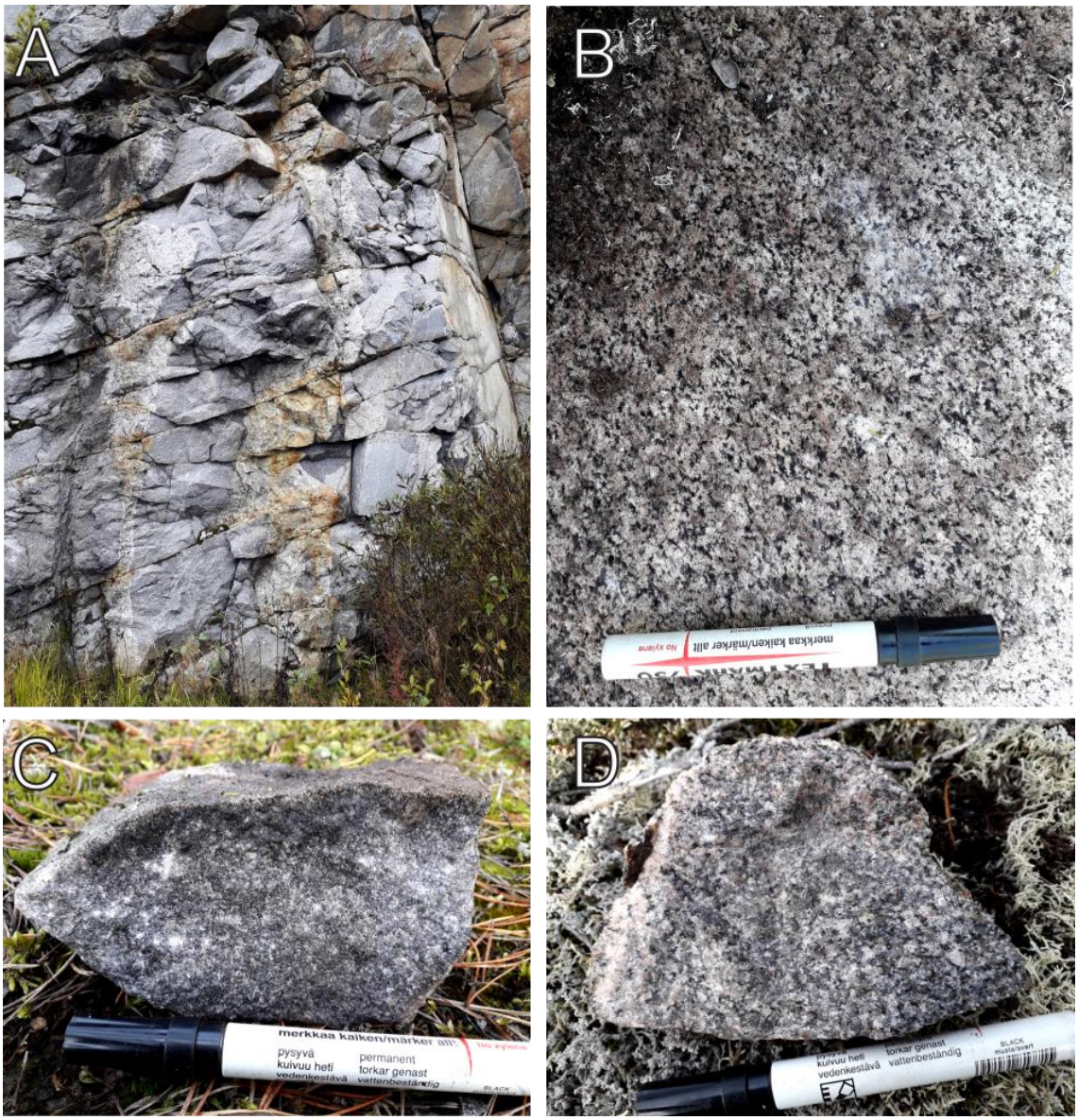

Figure 5. Characteristic intrusive rocks of the study area. A) Light grey medium-grained Nauriskallio tonalite with intersecting pegmatite dykes and subhorizontal jointing. The height of the rock wall in a construction aggregate quarry in Nauriskallio is 5 meters. TJLE-2020-77. B) Weathered surface of the massive tonalite near the contact of mica schist in the western part of Aukeannevankangas. TJLE-2020-65. C) Biotite rich and K-feldspar poor tonalite with small grain size in NE-part of Nauriskallio intrusion. TJLE-2019-104. D) Medium grained tonalite sample taken from the northern part of Nauriskallio intrusion. Notice the larger grain size and higher K-feldspar content than in TJLE-2019-104. TJLE-2019-103.

4.1.3. Dykes

The pegmatites in the study area are coarse grained (5 – 50 mm) and mainly consist of K-feldspar, plagioclase, muscovite and biotite. Tourmaline is also very common mineral in the pegmatites in the study area (*Fig. 6e*). Garnet and apatite occur in few outcrops. The pegmatites are either light grey or red, based on the feldspar composition. Both variants are very common throughout the lithologies in the study area. The pegmatite dykes are tens of meters long and the width of the dykes varies from few centimeters to few meters, usually somewhere between 20 and 40 centimeters (*Fig. 6b*). In addition to pegmatites, some fine-grained aplite and granite dykes are present in the study area. They are typically smaller and thinner than pegmatites, ranging from 1 to 25 centimeters in width.

Figure 6. Characteristic dykes of the study area. A) Pegmatite dyke subparallel to the foliation in a fine grained mica schist with sulphide graphite rich interlayers. TJLE-2020-19 B) 35cm wide pegmatite dyke in a fine grained mica schist. TJLE-2020-1. C + D) 5cm thick tourmaline pegmatite which is parallel to the foliation in a metagreywacke. TJLE-2020-43. E) Typical coarse grained pegmatite in the study area; feldspar, quartz, muscovite and tourmaline. TJLE-2020-46. Pen, rock hammer head and compass pointing north.

4.2. Deformation structures

The deformation structures in the study area are generally rather weak, but different foliations, folds and mineral lineations can be distinguished in most rocks. Primary structures are preserved throughout the study area and clear gneissic textures in supracrustal rocks are rare.

4.2.1. Primary structures

Primary bedding (S0) is widely visible in the supracrustal rocks of the study area (*Fig. 7a*), but bedding cannot be distinguished in the sulphide and graphite rich supracrustal rocks. Bedding in mica schists can be seen in thin sections as an increase of grain size and the amount of biotite. The more biotite rich layers indicate layers with pelitic origin whereas the psammitic layers contain much less biotite with significantly smaller grain size (*Figs. 7d, 7e*).

Concretions also usually follow the strike of the primary bedding because the concretions are typically bound to specific layers in supracrustal rocks.

Graded bedding and load casts are visible in some layers of the mica schists. These primary structures were exploited in determining the younging direction of the sedimentary sequences of the supracrustal rocks. The graded bedding and the coarsening of the grain size can be seen in *figure 7c*.

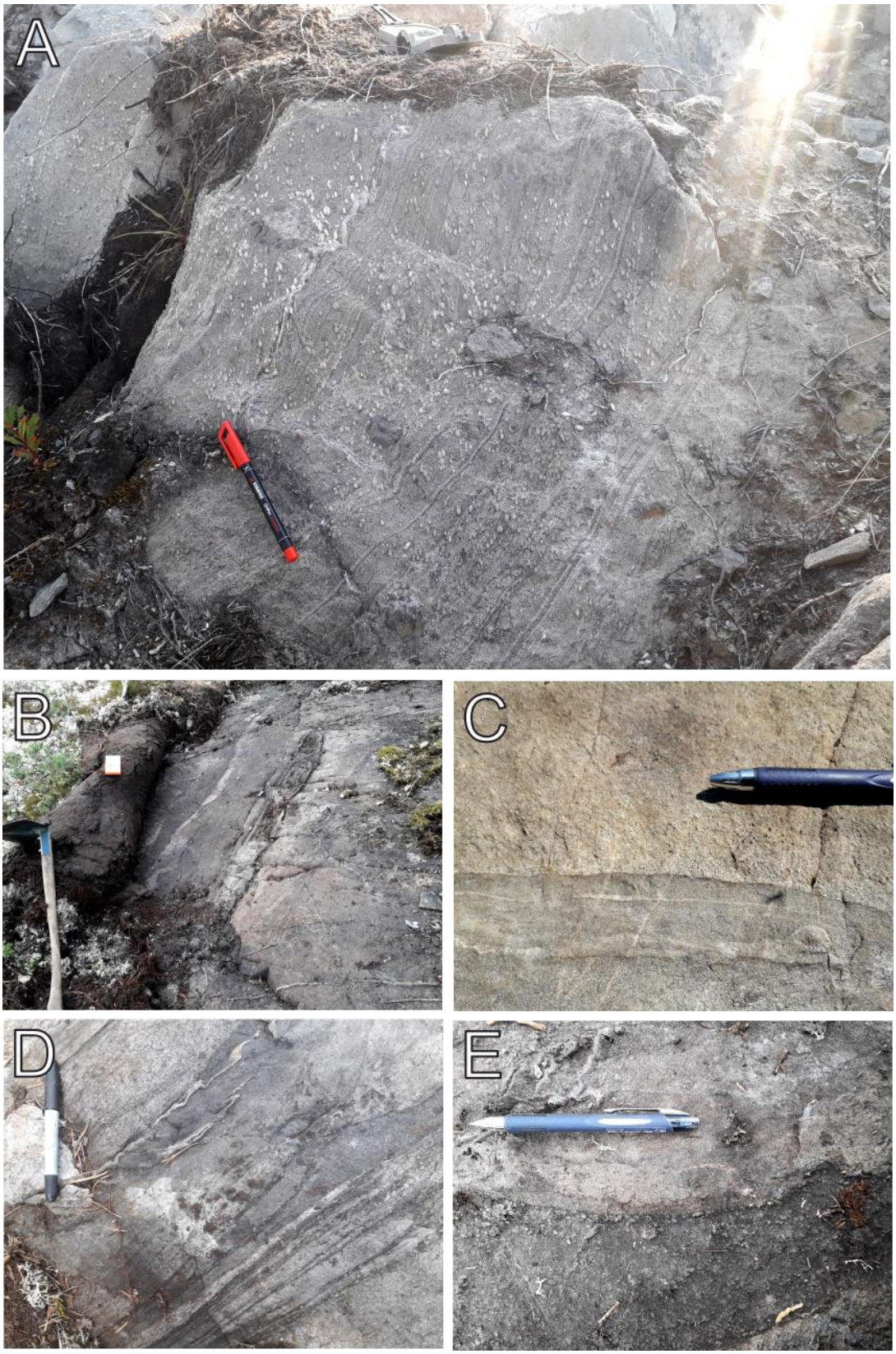

Figure 7. Primary structures on metasedimentary rocks of the study area. A) Primary bedding and elongate sillimanite porphyroblasts in a layered mica schist. TJLE-2020-15. B) Elongated calc-silicate concretion in metagreywacke. The quartz veins are abundant in the psammite layer. TJLE-2020-57. C) Graded bedding visible in the psammitic layer in mica schist. The darker layer at the bottom part of the picture is a pelitic layer. TJLE-2020-35. D) Folded quartz veins parallel to the bedding. Porphyroblasts are concentrated in the pelitic layers. TJLE-2020-64 E) Variation of pelitic and psammitic layers in mica schist. The porphyroblasts occur in the darker, pelite layer. Most of the quartz veins are present in the psammite layer. TJLE-2020-57. Pen is pointing north.

4.2.2. Deformation fabrics

Foliations

The most characteristic structural feature of the study area is the large fold-shape structure which can be seen in the aerogeophysical data. Different phases of the deformational evolution of the study area can be distinguished in the supracrustal outcrops of the study area and are related to the aforementioned fold.

The foliations in the supracrustal rocks of the study area are due to the parallel orientation of the biotite and muscovite grains. The foliations visible on outcrops can be divided in three different types. First, the strongest schistosity is the NE-SW and E-W trending schistosity which is commonly the most significant feature in the supracrustal rocks at the western and central parts of the study area (*Fig. 9a*). In the sulphide and graphite rich mica schists, this strong schistosity is typically the only structure visible at the outcrop scale (*Fig. 11b*). This foliation typically cuts the primary bedding and encloses the mineral lineation observed from quartz veins (*Fig. 8b*). South from the Aukeannevakangas intrusion, strongly foliated pelite layers occur with massive psammite layers (*Fig. 9b*). In the mica schists further away from the sulphide graphite schist, at the western part of the study area, this NE-SW schistosity is weaker, and can only be seen in the pelite rich layers (*Fig. 8a*). Dominating E-W schistosity crenulates older NW-SE and NE-SW schistosities north from the black schist (*Fig. 10a*).

Secondly, the NW-SE schistosity is usually weak, and it can be seen for example in the mica schists at the northern part of the study area. Here, this schistosity is weakly visible in only some of the layers and it contrasts with stronger and penetrative E-W foliation, which crenulates the NW-SE schistosity (Fig. *10b*). In Vattuaho this schistosity is the only schistosity visible in the outcrops (*Fig. 12c*).

Thirdly, the foliation parallel to the primary bedding is usually only visible in thin sections (*Fig. 20*).

The intrusions are normally massive, but the biotite grains display a planar alignment in some parts of the intrusions. This foliation is present especially close to the contact of the tonalite and the sulphide graphite schist at the eastern and the southeastern part of the Aukeannevankangas tonalite intrusion. At the northwestern and the southwestern parts of

the Aukeannevankangas tonalite the orientation is very weak and in many parts of the intrusion the orientation cannot be seen at all.

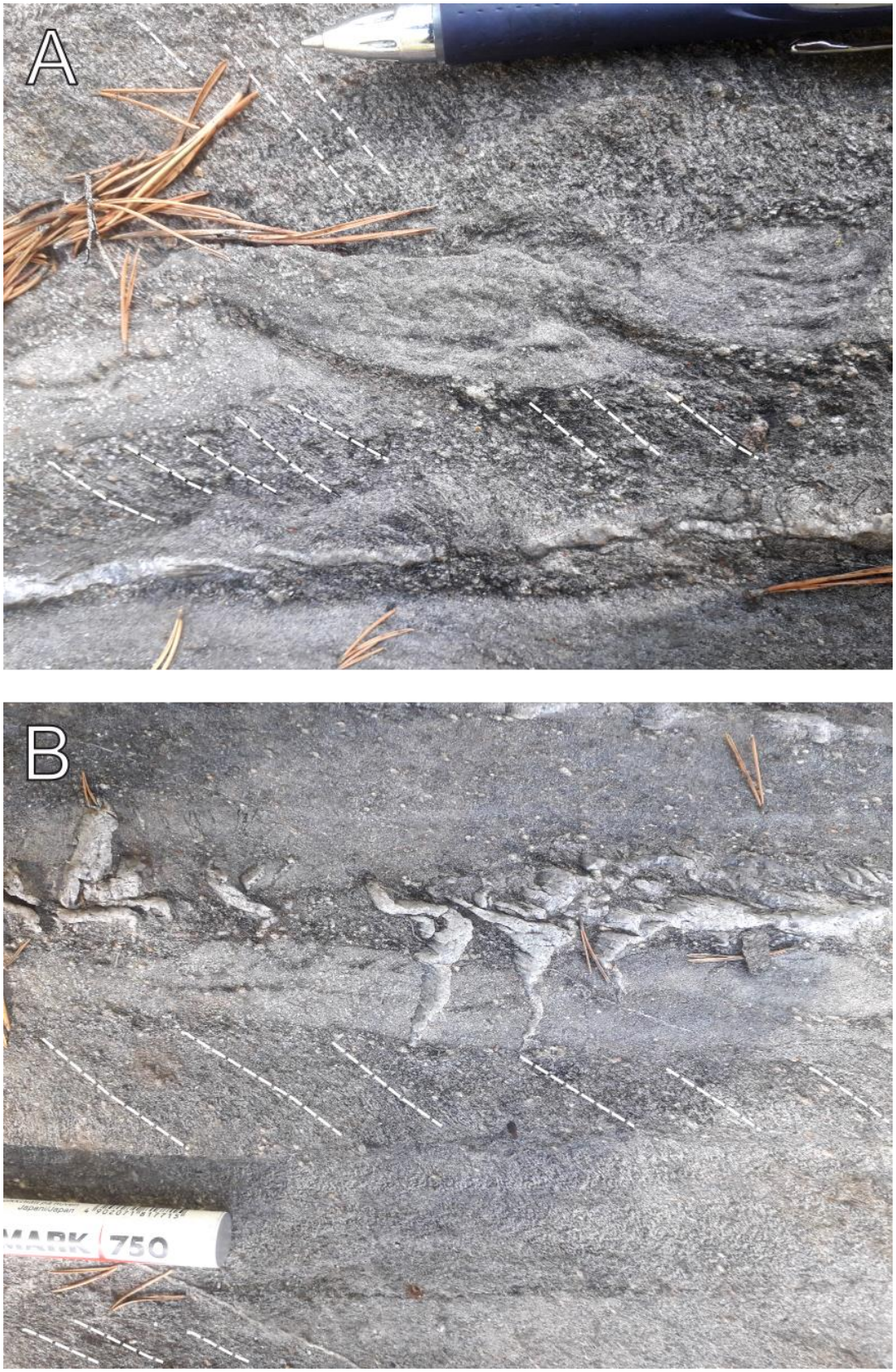

Figure 8. A) Weak NE-SW trending foliation which is distinguishable in pelitic layers. TJLE-2020-2. B) Primary bedding and crosscutting weak foliation in porphyroblast bearing metapelite. Mineral lineation plunging along the foliation plane can be seen in the folded quartz veins. TJLE-2020-2. Pen pointing north.

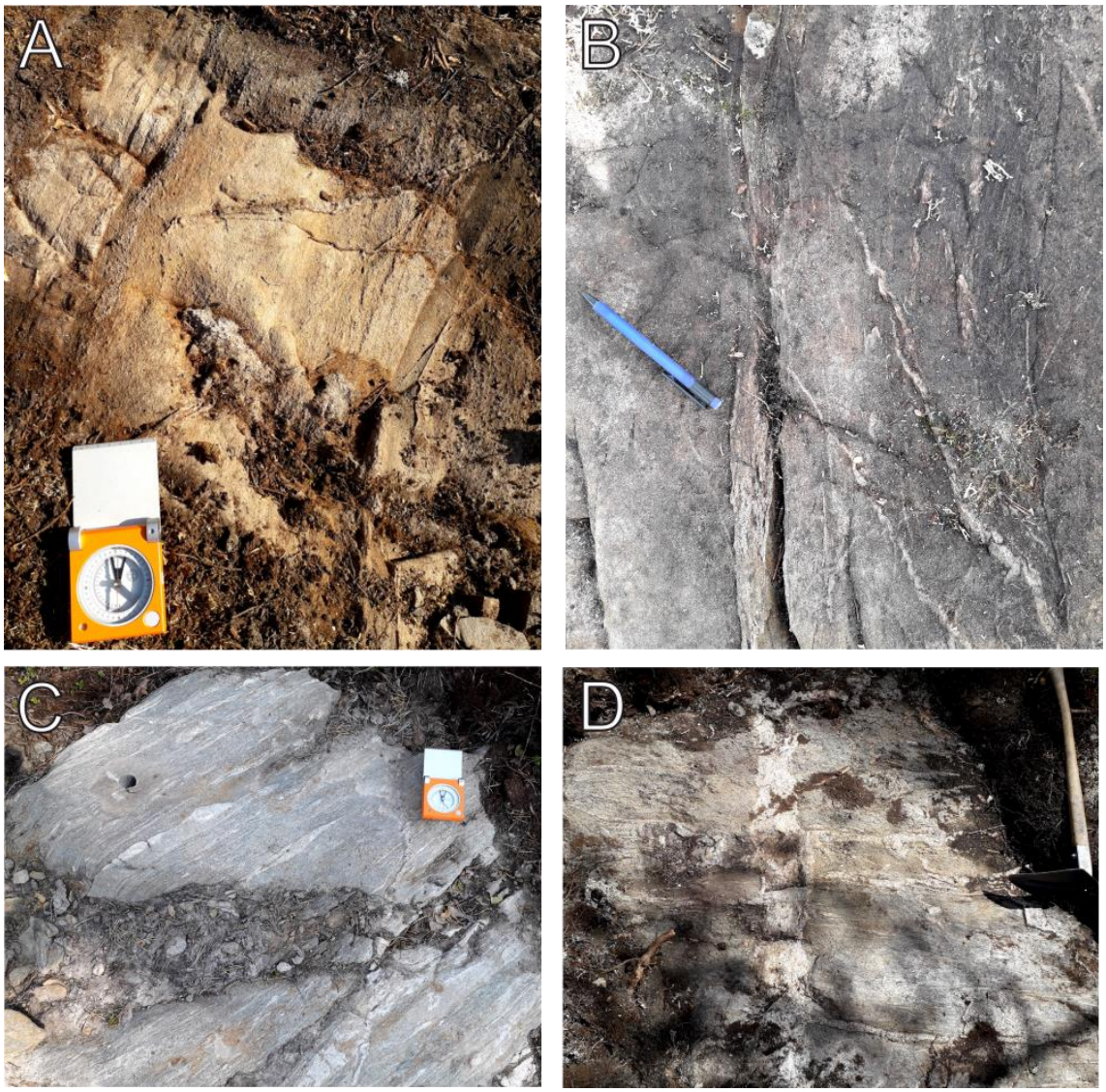

Figure 9. A) Moderate intensity, NE-SW trending foliation parallel to S0. TJLE-2020-22. B) Massive psammitic layers left and right in image and a strongly foliated (NE-SW) pelite layer center in image. TJLE-2020-42. C + D) Strongly oriented mica gneiss. The strong foliation is NE-SW trending. C: TJLE-2020-23. D: TJLE-2020-41. Pen, hoe and compass pointing north.

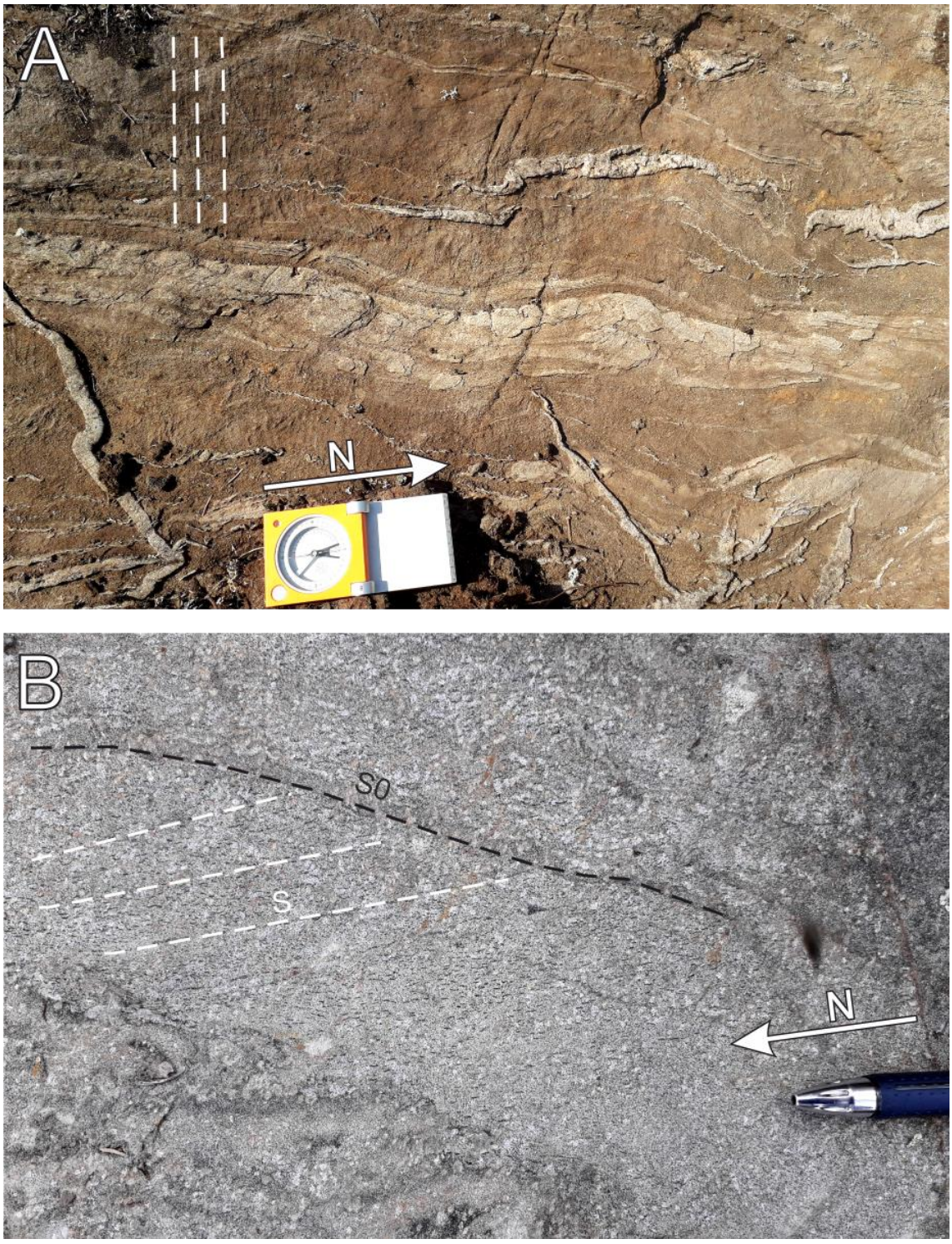

Figure 10. A) Open S-symmetric folding in a layered mica schist. Localized and weak axial plane schistosity and an intersecting E-W crenulation cleavage which have been developed in the mica rich layers of the rock (a white dashed line in the picture). TJLE-2020-26. B) Old weak NW-SE trending schistosity which can be seen in some layers of the mica schist. TJLE-2020-34.

Figure 11. A) Moderate E-W trending foliation. TJLE-2020-31. B) Strong E-W trending foliation in a graphite sulphide schist. TJLE-2020-11. C) Penetrative E-W trending foliation and syntectonic porphyroblasts in a mica schist. TJLE-2020-33. Pen and rock hammer head pointing north.

Folding & mineral lineations

Some supracrustal bedrock outcrops show folding of the primary bedding but this is not common in the study area. Examples of local folding of the supracrustal primary bedding can be seen at Pesämaankangas (*Fig. 12a & Fig. 12b*). The folding in Pesämaankangas is asymmetric and plunging, with axal planes dipping steeply towards west (268/68). Here, the fold hinges are rounded and the amplitude of the folding equals the wavelength. The fold axis measured in Pesämaankangas plunges gently towards south (169/25) which differs from the orientation of the larger scale SW-plunging Mansikka-aho synform (*Section 5.1*).

The relationship between the folding and the foliation is visible in Vattuaho (*Fig. 12c*). Here, the folding is open because the amplitude of the folding is small compared to the wavelength and the axial planes dip steeply towards SW.

All the mineral lineations observed during the summers 2019 and 2020 are measured from the quartz veins. The mineral lineation is typically due to recrystallization of quartz.

Figure 12. A) Folded primary bedding and intersecting axial plane schistosity in a contact zone of mica schist and tonalite. TJLE-2020-7. B) Hinge zone of an asymmetric fold with a fold axis orientation to the south in a mica gneiss. Picture towards north. TJLE-2020-7. C) Folded primary bedding planes in mica schist in Vattuaho. Quartz veins are parallel to the axial plane schistosity. TJLE-2020-15. Rock hammer head and compass pointing north.

4.2.3. Dykes, veins & joints

The quartz veins are often planar and cut the structures of the host rock, but quartz occurs also as irregular lenses or veins parallel to the bedding or schistosity. At least two generations of quartz veins are present in the supracrustal rocks of the study area. It is typical for quartz veins to occur within the psammite layers. The pelite rich layers also host quartz veins but these veins are usually thinner, and they occur more sparsely. At some outcrops, the veins sharply die out as the lithology changes from pelitic to psammitic in composition. When there are two populations of quartz veins present at the outcrop, the veins tending to have an E-W strike are typically wider than the N-S striking ones. These wider E-W veins usually cut the N-S striking veins which are typically parallel to the foliation. E-W-trending arrays of sinistral en echelon veins are sometimes present at the northern part of the study area. *Figure 14b* is an example of a quartz vein stockwork where younger veins are parallel to the foliation and the fold axes of the older veins plunge along the foliation plane. It is common to observe small-scale folding of the quartz veins which cut through the supracrustal rock units. The older generation of the quartz veins have folded on the later deformational events which have formed other distinct planar and linear features in the outcrops. The symmetry of folding is visible for example at Varsakalliot (*Fig. 10a*; TJLE-2020-26), where S-symmetric quartz veins occurs in a layered mica schist.

Usually the pegmatites, aplites and granite dykes are planar, crosscutting the lithologies and the planar structures, but minority of the dykes are folded. Many of the dykes are parallel or sub parallel to the trend of the foliation or the primary bedding (*Fig. 6a, 6c, 6d*). Similar to the quartz veins, the pegmatite dykes have a correlation with the width and the orientation in the supracrustal rocks. The dykes with more E-W strike are wider than the foliation-parallel dykes with N-S strike. The pegmatite, aplite and granite dykes show very limited evidence for internal deformation.

The most important outcrop in terms of joint observations is the Nauriskallio quarry. The tonalite of Nauriskallio is characterized by gently dipping subhorizontal joints, which seem to control and bound at least some of the dykes in the intrusion. In *figure 13b*, the bottom part of the wide tourmaline bearing pegmatite dyke is bounded by a subhorizontal joint.

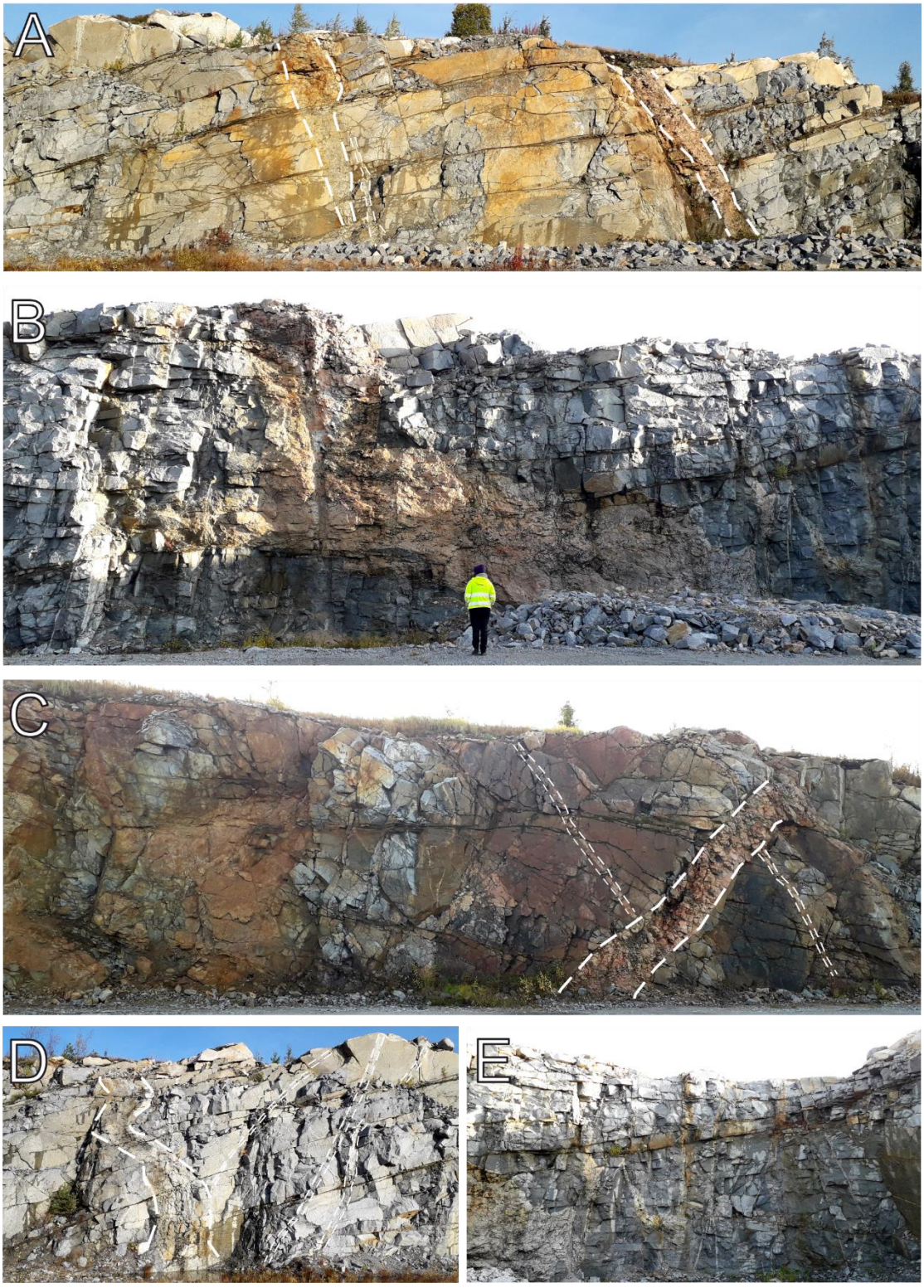

Figure 13. Overview of the pegmatite dykes and joints in a construction aggregate quarry in Nauriskallio. A) Steeply dipping pegmatite dykes in medium-grained massive tonalite in Nauriskallio. The tonalite is characterized by a gentle dipping subhorizontal jointing. The picture is towards NW and the height of the rock wall is 8 meters. TJLE-2020. B) Tourmaline rich pegmatite dyke bound in the left part of the photo by the subhorizontal jointing. The picture towards NE. C) Steeply dipping pegmatite and thinner, intersecting and stepping pegmatite dyke. Picture towards S. D + E) Pegmatite dykes in a tonalite which is characterized by subhorizontal jointing. D: Picture towards NE. E: Picture towards NE. Pictures taken in Nauriskallio construction aggregate quarry. TJLE-2020-6.

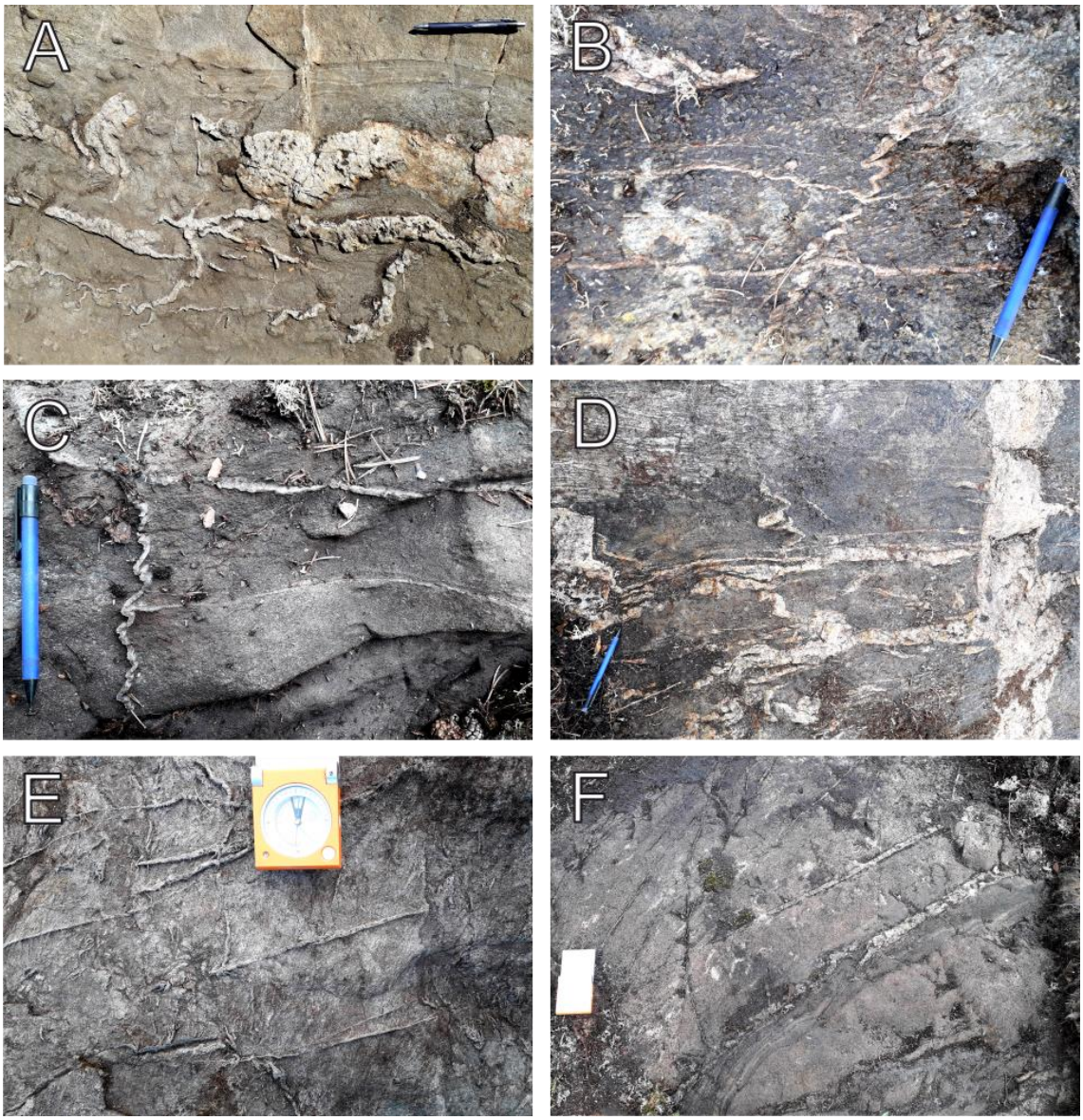

Figure 14. Relationships of the quartz veins and structures in mica schists. A) Quartz veins subparallel to the bedding in mica schist. TJLE-2020-35. B) Elongated porphyroblasts and two generations of quartz veins in metagreywacke. TJLE-2020-41. C) Quartz veins parallel to the foliation and folded quartz veins with fold axis plunging towards SW. TJLE-2020-53. D) Pegmatite dyke cutting a strongly foliated metagreywacke. The outcrop is full of quartz veins; younger veins are parallel to the foliation and older veins are folded with fold axis plunging along the foliation planes. TJLE-2020-41. E) Two generations of quartz veins in mica schist. TJLE-2020-30. F) Mica schist with wider quartz veins parallel to S0 and thin quartz veins parallel to S. The foliation is penetrative and the layers have graded bedding which indicates top to the west. TJLE-2020-44. Pen and compass pointing north.

4.3. Thin sections

4.3.1. Supracrustal rocks

Mica schists

Based on the thin section study, the ground mass of the supracrustal mica schists is composed mainly of fine grained (0,1 mm – 0,2 mm) biotite and quartz. Small amounts of muscovite and plagioclase grains are visible in the ground mass. The biotite grains are oriented in a parallel arrangement and define the prevailing foliation. The quartz grains are weakly or moderately rounded and it is typical for quartz grains to have undulose and zonal extinction when studied under cross polarized light.

The bedding in mica schists can be seen in thin sections as an increase of grain size and the amount of biotite. The more biotite rich layers indicate layers with pelitic origin whereas the psammitic layers contain much less biotite with significantly smaller grain size.

Porphyroblasts are common especially in the layers with pelitic origin. At the psammitic layers, the porphyroblasts are less common and their grain size is smaller. Four types of porphyroblasts are present in the mica schists. The largest and macroscopically easily visible porphyroblasts are usually fibrous sillimanite (i.e. fibrolite). These brown fibrolite porphyroblasts do not have inclusions. It is very common that fibrolites have been altered to muscovite. This alteration usually takes place at the grain boundaries, dominantly within clay rich layers and is much less common in the psammitic layers.

Large andalusite porphyroblasts can be found from the study area (*Fig. 15a*). Andalusite blasts have a really large number of biotite, quartz, and muscovite inclusions. Muscovite alteration of andalusite is common and it has sometimes advanced to a point where andalusite is barely recognizable.

Poikiloblastic K-feldspar porphyroblasts occur in mica schists. The grain size of the K-feldspar poikiloblasts varies from 0,2 mm to 0,5 mm. Poikiloblasts contain large number of inclusions which are mainly quartz, biotite, and muscovite.

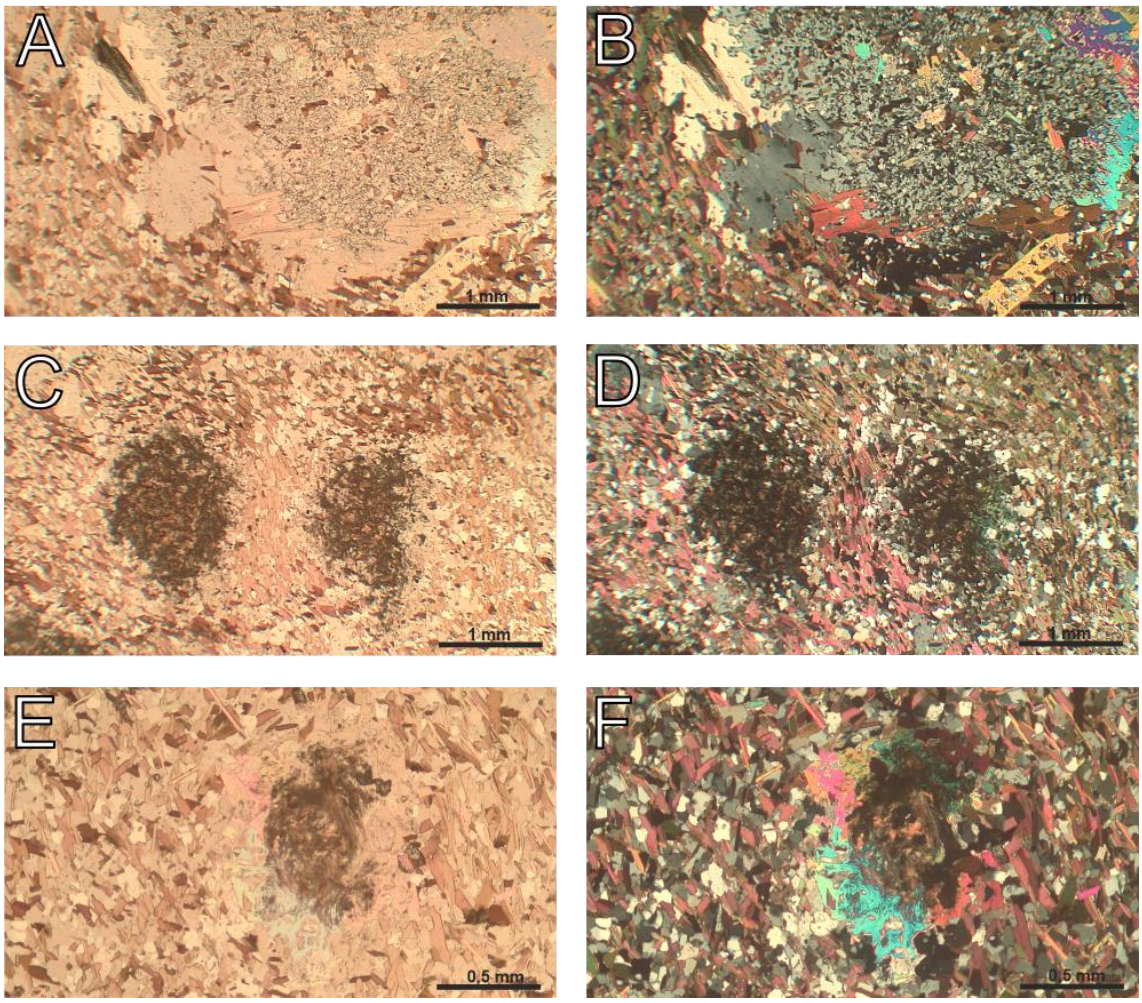

Figure 15. Photomicrographs of andalusite and sillimanite porphyroblasts in mica schists. The pictures on the left are taken in plane polarized light (PPL) and the pictures on the right are taken in cross polarized light. North is upwards in every picture. A) Large pre or early-syntectonic andalusite porphyroblast which is full of inclusions. Alteration to muscovite is visible at the right margin of the porphyroblast. Andalusite does not have an internal foliation. The yellowish mineral in cross polarized light near the bottom right corner is posttectonic muscovite. TJLE-2020-32.2. B) Syntectonic fibrous sillimanite (i.e., fibrolite) porphyroblasts. The foliation strongly deflects around the porphyroblasts. TJLE-2020-15.1. C) Sillimanite has been altered to muscovite. The alteration starts at the margins of the porphyroblast. TJLE-15.2.

The grain size of muscovite porphyroblasts varies from slightly coarser than the groundmass up to 1 millimeter. The abundance of muscovite porphyroblasts varies throughout the studied samples. Occasionally fibrous sillimanite and fine sillimanite needles can be distinguished in the center of the muscovite blasts. Inclusions are typical in the muscovite porphyroblasts and occasionally muscovite has poikiloblastic texture, when the blasts are completely full of quartz, biotite and opaque inclusions (*Fig. 16f*; TJLE-2020-32).

Fibrolite porphyroblasts are typically elongated in the direction of the foliation. The external foliation commonly wraps around the porphyroblasts of sillimanite, but the

intensity of this deflection is variable across the study area. The deflection of foliation around the porphyroblasts vary from weak (*Fig. 16a*; TJLE-2020-2) to strong (*Fig. 16b*; TJLE-2020-15).

The internal foliation of the K-feldspar porphyroblasts within the studied thin sections is generally parallel with the external foliation (*Fig. 16c*; TJLE-2020-2), while the andalusite blasts have no distinct internal foliations. The foliation does not deflect around the andalusite porphyroblasts. (*Fig. 15a*; TJLE-2020-32).

Muscovite blasts cut the underlying fabric sharply and show clear posttectonic character.

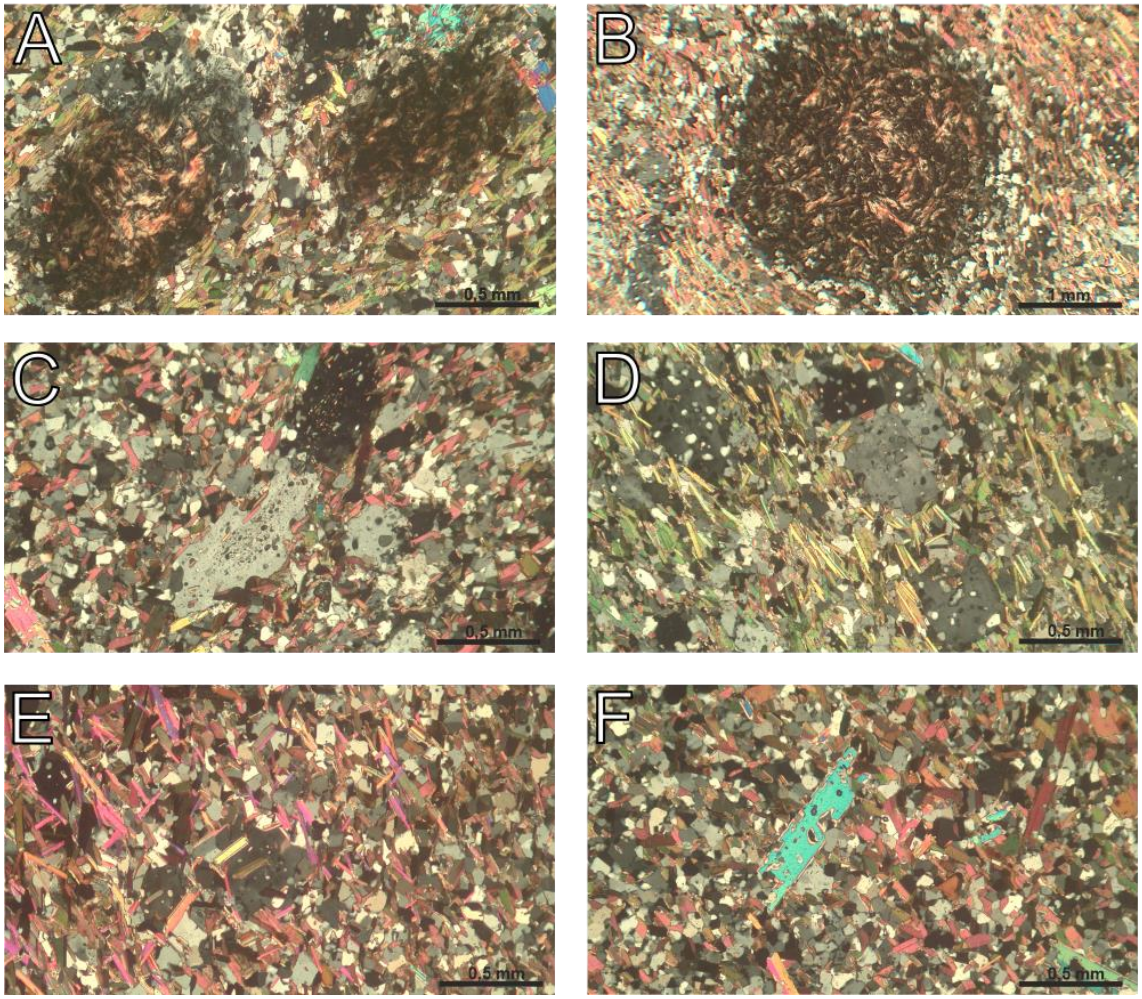

Figure 16. Photomicrographs of the relationships of the metamorphic porphyroblasts and external foliations. All the pictures are taken in cross-polarized light. North is upwards. A) Syn-/latetectonic fibrolite porphyroblasts. The porphyroblasts are elongated parallel to the NE-SW foliation. TJLE-2020-2.1. B) Pre-/earlytectonic fibrolite porphyroblast. The deflection of the foliation around the porphyroblast is strong. TJLE-2020-15.1. C) Late-/posttectonic poikiloblastic alkali feldspar porphyroblast. Internal foliation of the blast has one orientation which is parallel to the stronger external foliation (NW-SE). There is also another orientation of the external foliation (E-W). TJLE-2020-2.2. D) Late-/posttectonic poikiloblastic alkali feldspar porphyroblasts with internal foliation at random orientation. TJLE-2020-15.1. E) Posttectonic muscovite porphyroblasts. TJLE-2020-15.2. F) Coarse grained posttectonic muscovite poikiloblast. TJLE-2020-32.3.

Black schists

The distinct difference of the black schist interlayers versus the normal supracrustal mica schist, comprising quartz, plagioclase, biotite and muscovite, are the very fine graphite grains and sulphides which appear throughout the thin section samples (*Fig. 17a*). The maximum grain size of the graphite is approximately 50 microns. The opaque minerals vary in size, but the largest also macroscopically visible grains are up to 1 mm. Distinct for the black schists are yellowish patches which occur throughout the samples, which result from sericite and pinite alteration which usually takes place in the K-feldspar poikiloblasts. Alteration products have started to occupy the feldspar grains from the grain boundaries and joints. The muscovite occurs also as an alteration product of the K-feldspar blasts. The degree of the sericite alteration is much higher in the black schists than in the normal mica schists. Some sillimanite porphyroblasts have gone through a total sericitization. Special feature in the black schists of the southern limb of the Mansikka-aho synform is a euhedral garnet which seem to be rare in the study area.

Syn- or latetectonic K-feldspar poikiloblasts and fibrous sillimanite, and posttectonic muscovite porphyroblasts can also be found in the black schist layers. The black schist samples show signs of high strain, as the orientation is strong and the sillimanite porphyroblasts are strongly elongated towards the direction of the foliation (*Fig. 17b*).

4.3.2. Intrusions

Aukeannevankangas intrusion

The samples from the Aukeannevankangas intrusion are coarse grained with mineral composition of mostly quartz, plagioclase and K-feldspar. The K-feldspar content of 10-20 % indicates that the intrusion is granodiorite (*Fig. 17c*; TJLE-2019-101.2). The samples contain also coarse biotite grains, which have commonly been altered to chlorite. The biotite grains in the thin section samples of Aukeannevankangas do not display a preferred foliation.

Nauriskallio intrusion

The samples of the Nauriskallio intrusion contain high amounts of plagioclase compared to K-feldspar (*Fig. 17d*; TJLE-2019-114.2). The Nauriskallio intrusion is a tonalite,

which has a distinguishable foliation which can be seen both macroscopically and microscopically as an SW-NE alignment of biotite grains. The chloritization of biotite is common in the Nauriskallio samples.

Hautamaa intrusion

The Hautamaa intrusion (*Fig. 18*) varies from massive to weakly oriented. The special feature of the Hautamaa intrusion is the porphyritic texture which is due to the presence of large K-feldspar grains (*Fig. 17e*; TJLE-2019-104.3). These porphyritic grains are full of quartz, biotite and plagioclase inclusions. Further, graphic texture, intergrowth of quartz and alkali feldspar, is visible in K-feldspar grains. Biotite has finer grain size than the Aukeannevankangas and Nauriskallio intrusions. The samples of the Hautamaa intrusion vary from granodioritic to porphyritic granite.

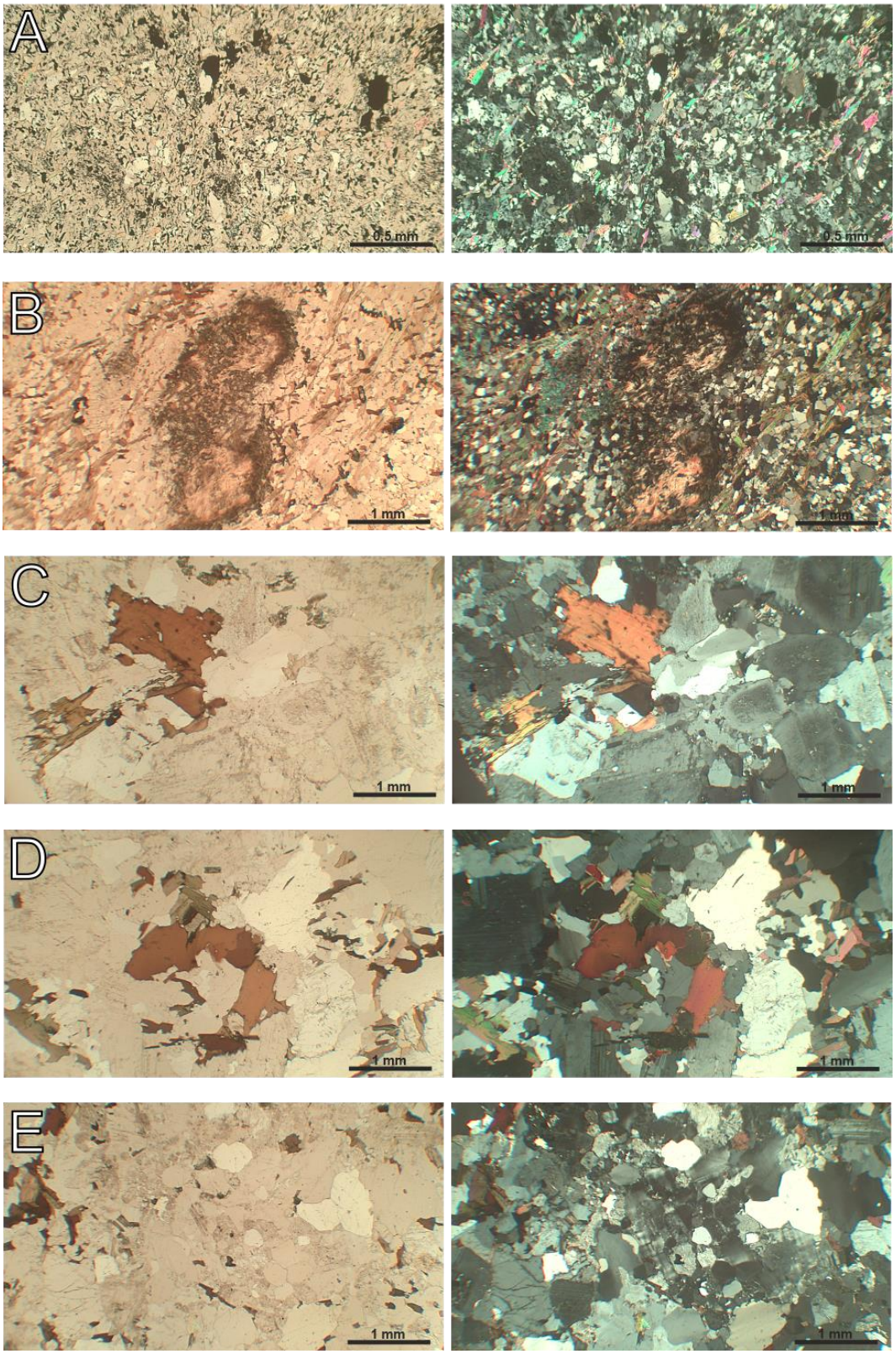

Figure 17. Photomicrographs of the black schists and intrusions in the study area. The pictures on the left are taken in plane polarized light (PPL) and the pictures on the right are taken in cross polarized light. North is upwards in every picture. A) A fine-grained black schist rich in graphite. TJLE-2019-90.2. B) A black schist with sillimanite porphyroblasts elongated towards the direction of the foliation. TJLE-2019-110.3. C) Massive Aukeannevankangas granodiorite. The chloritization of biotite is visible in smaller grains at the upper part of the picture. TJLE-2019-101.2. D) The biotite grains show signs of chloritization in Nauriskallio tonalite. The weak orientation of biotite is not visible in this picture. TJLE-2019-114.2. E) Hautamaa intrusion is characterized by porphyritic K-feldspar grains (the whole upper right part of the picture). TJLE-2019-104.3.

5. Structural interpretation & discussion

5.1. Structural geometry

Two major fold structures are interpreted in *figure 18*; the plunging Mansikka-aho synform at the northern part of the study area and the plunging Mansikka-aho antiform at the south. The measured fold axes cluster strongly towards SW with majority of the fold axes having plunges between 45 and 60 degrees (*Fig. 18*). The cluster of lineation data in the stereoplot is towards WSW (*Fig. 18*). Lineation plunges does not have much variation between the different parts of the study area. Majority of the lineation plunges are between 30 and 50 degrees. Lineation data supports the interpretation of the large-scale SW plunging antiforms and synforms. The mineral lineation and the mineral elongation follow the SW plunging pattern throughout the study area.

The plunges of fold axes are steeper towards the southern parts of the study area. Based on the lineation, bedding and schistosity data, the fold axis and the axial surface of the Mansikka-aho synform bend from NE-SW to E-W trend towards E.

Both limbs of the Mansikka-aho antiform are dipping towards northwest indicating that the antiform is overturned. The Mansikka-aho synform does not show similar overturned feature, but it is noteworthy that the planar structures of the synform are almost vertical. The observations of the younging direction of stratigraphy between old GTK observations and the observations taken in 2020 are somewhat conflicting in the eastern part of the area, but based on the newer observations taken in 2020, the stratigraphy is overturned in the synform.

In contrast to the available bedrock map by GTK, the new interpretation is that the Nauriskallio tonalite and the porphyritic granodiorite (at the area of Hautamaa) are two separate plutonic units. The processed, more detailed aeromagnetic map shows an intervening magnetic anomaly between the intrusions. This anomaly is higher than the intrusive rock and it does not contain any bedrock observations. The interpreted porphyritic granodiorite intrusion is verified by an outcrop surrounded by wetlands with no further bedrock outcrops. Furthermore, the differing mineralogy and the texture of the porphyritic granodiorite makes it justified to distinguish it from the Nauriskallio tonalite and consider it as a separate plutonic unit.

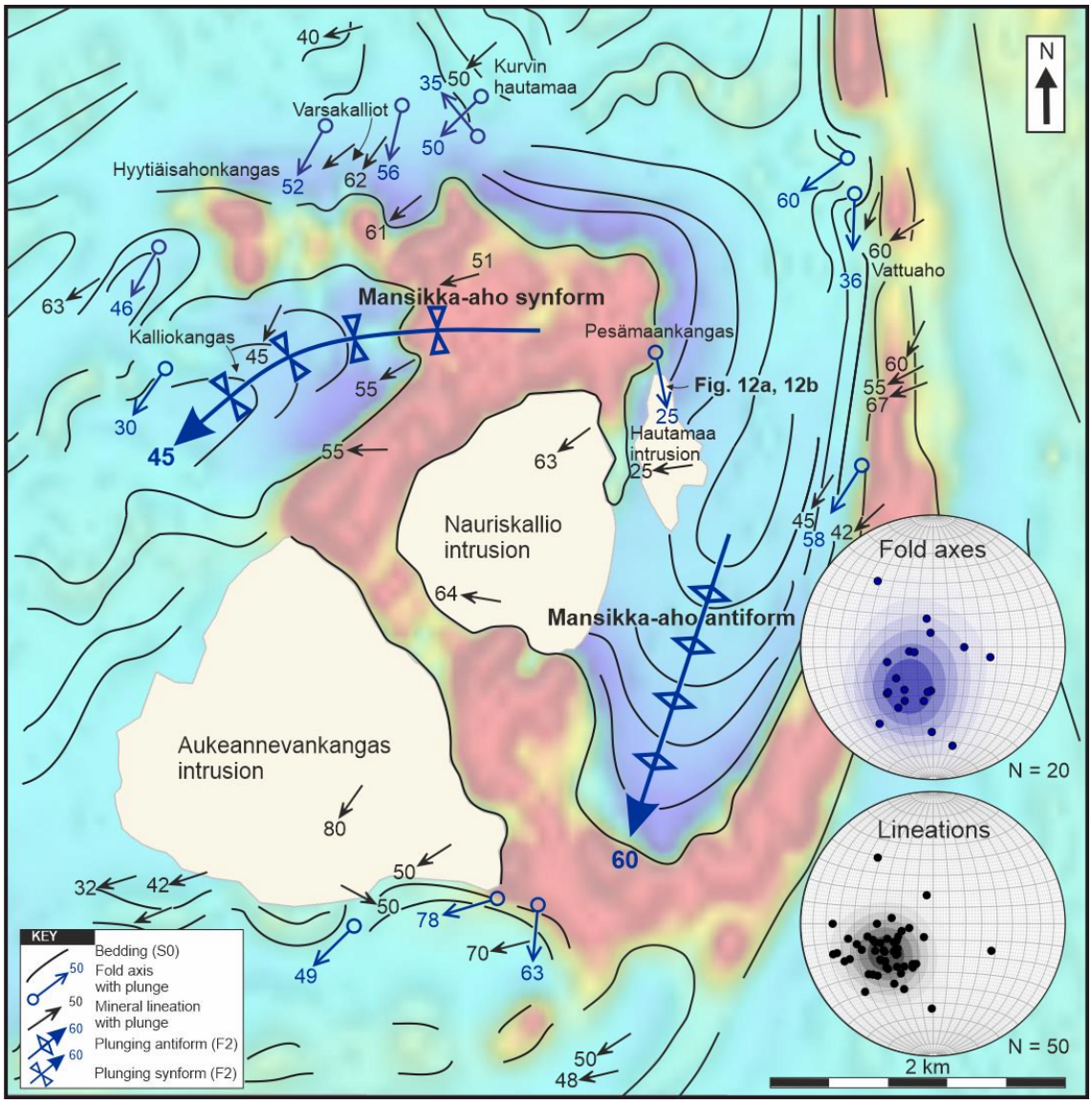

Figure 18. Structural geometry of the study area. Generalised map of the fold axes and the mineral lineations. Aeromagnetic map modified after Geological Survey of Finland.

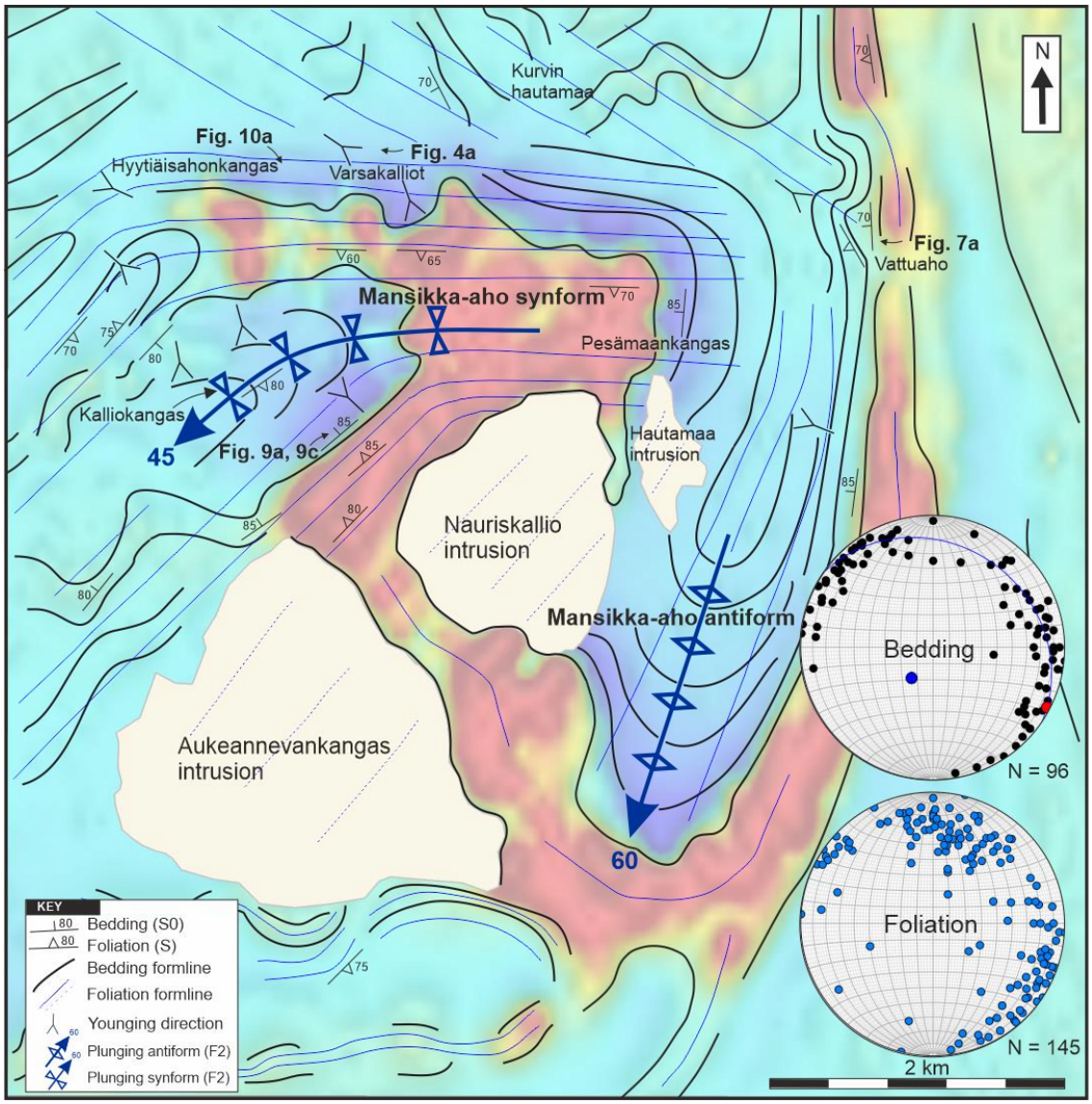

Figure 19. Structural interpretation of the study area. Maximum eigenvector (red dot), minimum eigenvector (blue dot) and the great circle normal to the minimum eigenvector (blue great circle) are included in the equal area spherical projection of the bedding data. Aeromagnetic map modified after Geological Survey of Finland.

Most of the observations of the younging directions of the stratigraphies indicate that the stratigraphy gets older towards the inner part of the Mansikka-aho synform (*Fig. 19*). Younging directions of the Mansikka-aho antiform are uncertain due to limited number of observations. The stratigraphical top observations are concentrated on the northern and center parts of the Mansikka-aho synform. The observations are lacking especially at the southern part of the study area, and the eastern part contain only some occasional observations.

5.2. Relative ages of the deformation fabrics

The age relationships of the different foliations were studied both at the outcrops and through thin sections. At least three generations of foliation can be found in the study area.

The foliation (S1) parallel to the bedding (S0) can be seen in thin sections (*Fig. 20*). At the southern parts of the study area, where primary layers have not been transposed as heavily as in the north, this foliation might be also visible in the field (*Fig. 9b*; TJLE-2020-4). This foliation may be a result of sedimentary compaction, but more likely due to isoclinal thrust systems occurred before the dominant foliation visible in most of the outcrops.

The northern parts of the study area are divided into areas characterized by the weaker and only at some places visible NW-SE foliation (S2) or easily visible NE-SW or E-W foliation (S3). S2 is noticeable at the northern limb of the Mansikka-aho synform (*Fig 10b*; Varsakalliot and Kurvin hautamaa) and at Vattuaho (*Fig. 12c*). It is uncertain if the interpreted S2 at the northern limb of synform represents a foliation generation of its own or is it the bedding parallel S1.

At Varsakalliot and Kurvin hautamaa the S0 tends to have NW-SE or N-S direction in contrast to the predictable E-W direction of the northern limb of the Mansikka-aho synform. This change or curve in the bedding direction might be related to the vicinity of the interpreted shear zones.

At Vattuaho, this NW-SE foliation (S2) is not parallel to the S0. Here, the NW-SE foliation is undoubtedly older than the NE-SW foliation which is recognizable only in posttectonic crystallization of muscovite in thin sections.

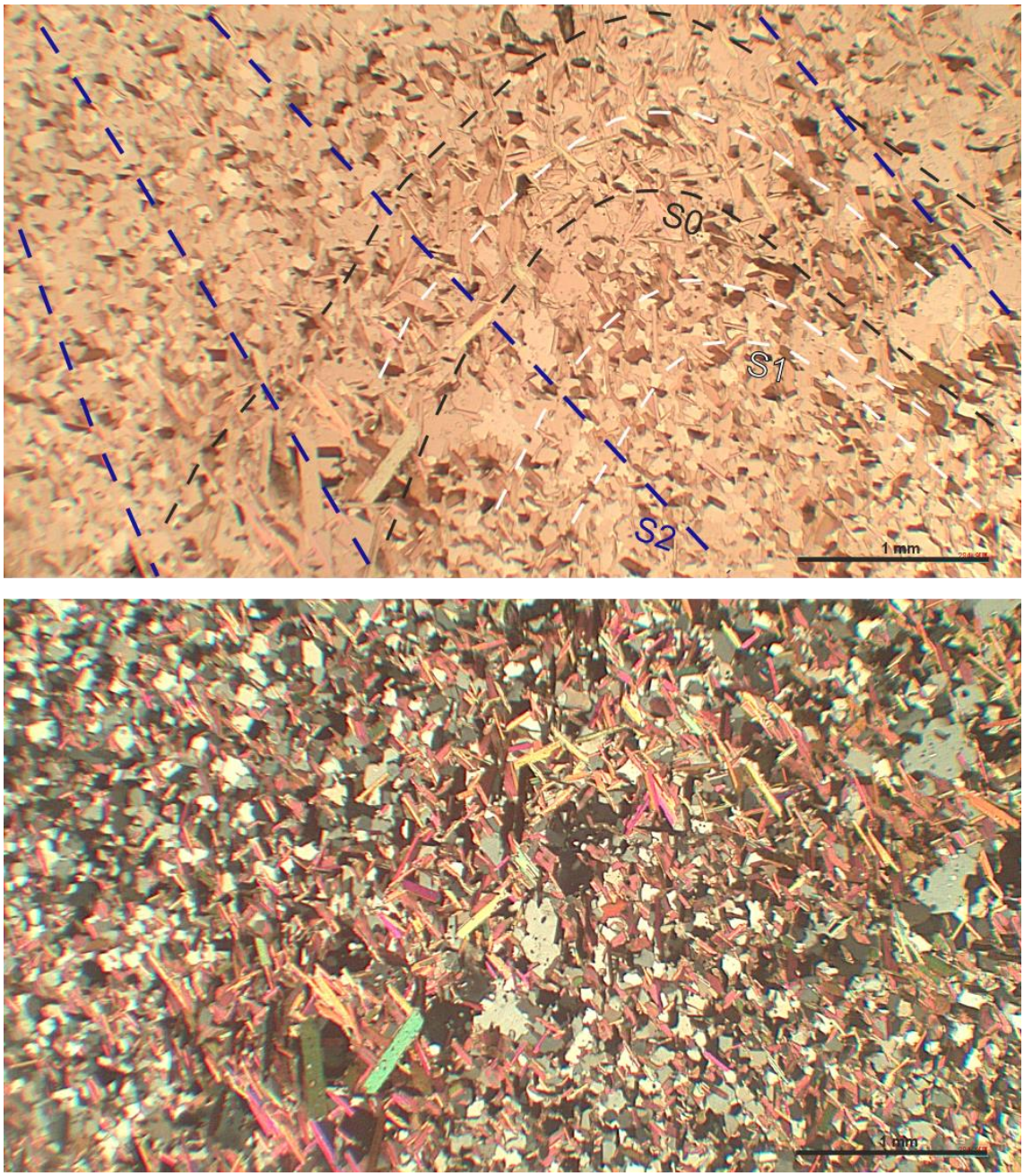

Figure 20. Bedding (S0) and two generations of foliation (S1 and S2). Plane polarized light and cross polarized light views of the same thin section. North is upwards. TJLE-2020-15.2.

5.3. Structural domains

The study area is divided in 4 structural domains (*Fig. 21*); domain 1 represents the northern limb of the Mansikka-aho synform. The S0 data is unclear in the central part of the domain. The bedding observations from the western part of the domain are fairly consistent with NE-SW strike. The dips are almost vertical, typically ranging from 80 to 90 degrees.

Domain 1 has two distinctive foliations: moderate to strong, younger E-W trending, south-dipping foliation at the southern part of the domain and a weaker, older NW-SE trending foliation. The dip direction of the older foliation is towards SW and the dips vary between 55 and 85 degrees.

The dykes and veins in domain 1 tend to have a trend towards NW-SE or E-W and a dip direction towards SW or S. The dips of these dykes and veins vary between 65 and 85 degrees. Most of the observed dykes or veins in this domain are quartz veins. The pegmatite and aplite dykes have dip directions towards SW and none of these dykes have E-W strike.

Domain 2 covers the inner part of the Mansikka-aho synform. The foliation in the domain 2 strikes from NE to SW, but it bends towards east at the northeastern part of the domain.

Most of the dyke and vein observations in domain 2 are quartz veins. The dips of the dykes and veins range from 75 to 90 degrees with dip directions spreading both NW and SE. The pegmatite data with dip directions and dips is limited, but they are dipping steeply towards NW.

Domains 3 and 4 comprises the Nauriskallio and Hautamaa (domain 3) and Aukeannevankangas (domain 4) intrusions. Majority of the dyke and vein observations are pegmatite and aplite dykes. The dykes and veins have two orientations with respect to the intrusions: parallel to the contact of the intrusion and the supracrustal rocks and perpendicular to the contact. The majority of the observed dykes locate within, or close to the contact zones, whereas the central parts of the intrusions largely lack dykes and veins. The dips of the majority of the dykes and veins in domain 2 vary between 45 and 75 degrees. The dip data in domain 3 is very limited but it contains dips which range from 70 to 85 degrees.

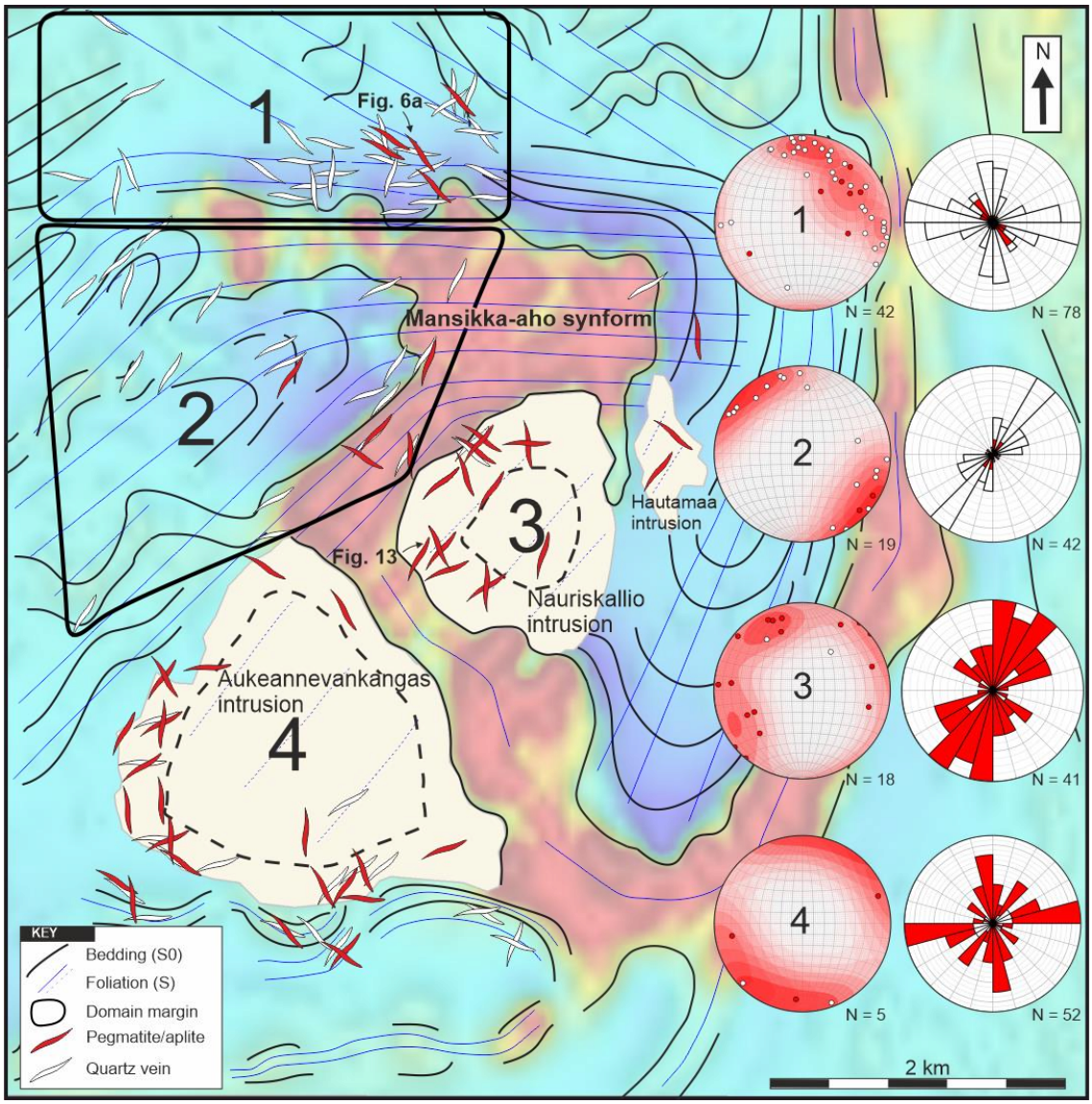

Figure 21. Generalised map of the veins and dykes in the study area. The dashed lines within the intrusions indicate the decrease in number of dykes and veins towards the center of the intrusions. Pegmatite dykes (red dots) and quartz veins (white dots) are presented in stereograms. The pegmatite dyke (red sectors) and quartz vein (white sectors) observations with only strike data are presented in circular histograms. Aeromagnetic map modified after Geological Survey of Finland.

5.4. Structural & tectonic evolution of the study area

When examining the aeromagnetic data and the lithological and structural context of the study area as a part of Ostrobothnia supracrustal schist belt, the study area seems to be part of a regional-scale open fold (*Fig. 22*). In this context, the Aho metavolcanic belt marks the eastern limbs of this regional fold. The western limbs of this regional fold are bounded by the Vaasa migmatite complex/Vaasa granite.

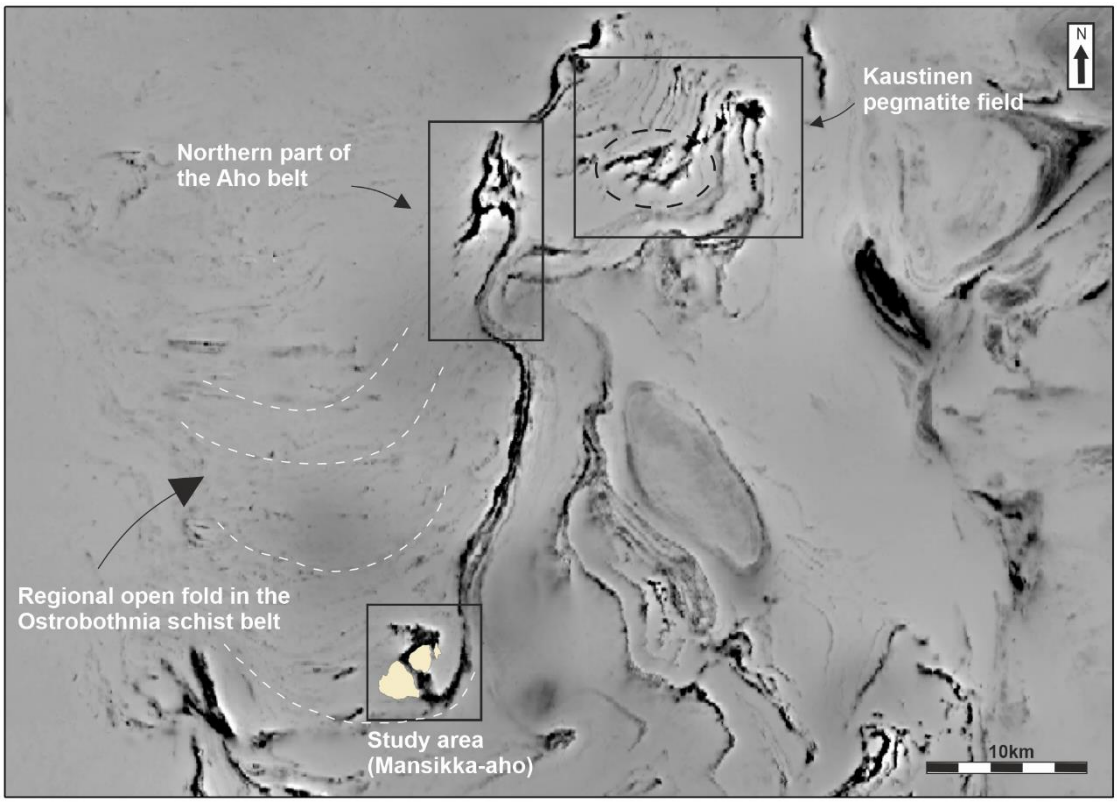

Figure 22. The study area as a part of Ostrobothnia schist belt and a regional open fold. The study area has similarities with structural frameworks of the northern part of the Aho belt and the Kaustinen area. Black dashed circle indicates the z-symmetric folding which is also present in the study area. Aeromagnetic map from the Geological Survey of Finland.

The observations related to kinematic indicators are lacking from the study area. The continuous negative NE-striking anomalies in aeromagnetic data are interpreted to be shear zones. One of these shear zones cuts the northwesternmost corner of the study area and continues bedding-parallel just west from the Aho metavolcanic belt (*Fig. 23; SZ 1*). Another low-magnetic area curves around the Mansikka-aho synform (*Fig. 23; SZ 2*). These shear zones are parallel with the NE-SW shear zone (*Fig. 23; SZ 3*) and a shear zone south from the study area which was interpreted by Vuorela (1982) and Veriö et al. (1993) (*Fig. 23; SZ 4*).

The interpretation of NE-striking shear zones fits well to the data where the intensity of the foliation is higher at the NE-striking structures. The deformation has a higher apparent intensity within structures occurring parallel to a shear zone. This can be well seen at the southern limb of the Mansikka-aho synform (*Figs. 9a, 9c*; TJLE-2020-22, TJLE-2020-23) where the intensity of foliation is generally moderate or strong, in contrast to the typically weak foliation in the study area. The northern limb of the Mansikka-aho synform is not parallel with the NE shear zone and consequently, the foliation is significantly weaker along the southern limb of the synform.

The shape of the magnetic anomaly of the supracrustal rocks of the study area can be explained by transpressional movement generated by NE-oriented shear zones north (*SZ 1*) and south (*SZ 4*) from the study area. The bedding planes of the regional open fold are possible weakness planes where shears have taken place. In this shear-bound block model the movement is clockwise, ie. dextral in relation to the southern boundary. The relative direction of movement along the central shear zone is sinistral.

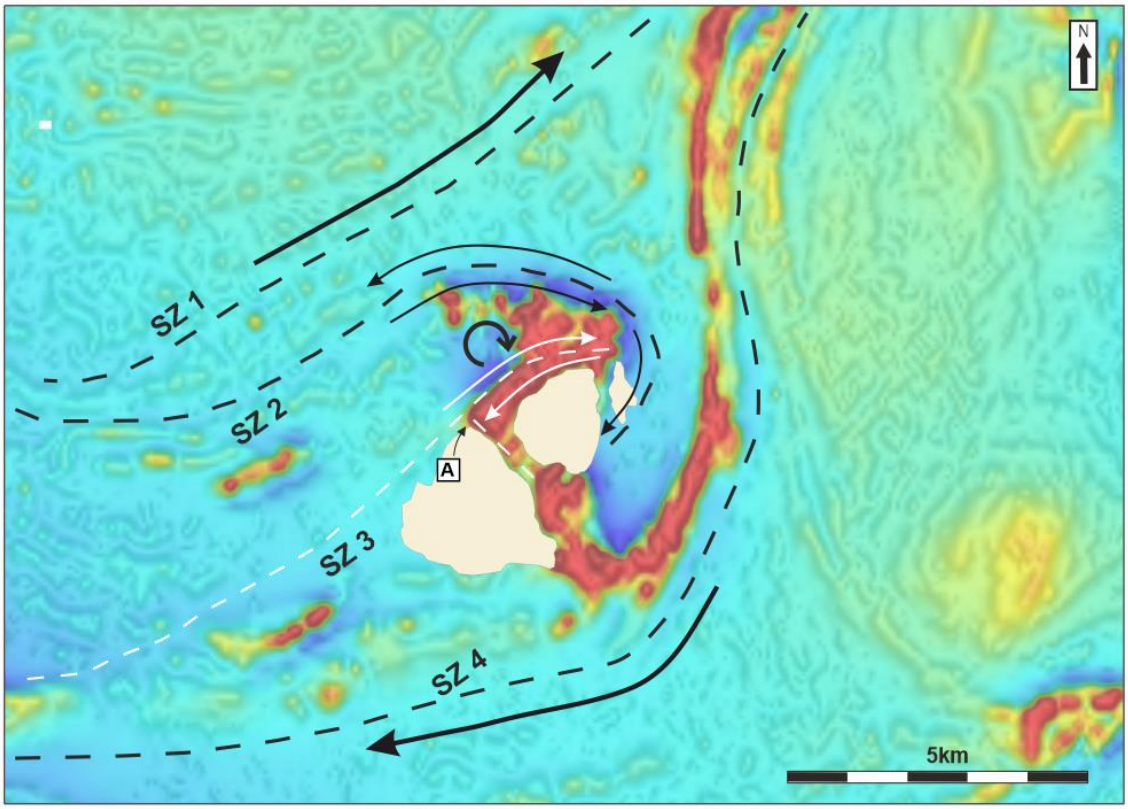

Figure 23. Interpreted shear zones (dashed lines) in the study area. Black arrows indicate the relative movement of the shear-bound blocks. "A" is a text reference from chapter 5.4. Aeromagnetic map from the Geological Survey of Finland.

For example, the NW-SE foliation in Vattuaho is related to the transpressional clockwise rotation of the study area and the shear zones generating it, or completely different tectonic event prior to this event. One possible explanation for this NW-SE foliation is the formation of the above-mentioned regional-scale open fold in Ostrobothnia schist belt (*Fig. 22*).

The near 90-degree bend from NW-SE to NE-SW of the high-magnetic supracrustal rocks at central part of the study area (*Fig. 23*; A) could be explained by multiple shear zones active at a same time, or activation of a new NE shear zone just north from the intrusions of the study area (*Fig. 23; SZ 3*). In this model the relative movement of this central shear zone is dextral.

This possible central *shear zone 3* hosts a natural space for the intrusion of the granitic magma. It is also possible that the earlier formation of the intrusions of the study area is related to this bent geometry of the high-magnetic supracrustal rocks at the central part of the study area. The results of the structural analysis support the idea that the bending of Mansikka-aho synform axis from NE to E happened approximately at the same time in the same event, so there was probably not enough time for the placement and cooling of the intrusions to take place between these events. The more probable explanation is that the intrusions were placed at another NE-SW trending shear zone which was the controlling factor in the bending of the fold axis towards the east.

Folding in three scales has taken place in the study area. The overturned stratigraphy means that the whole stratigraphy sequence has been inverted before the D2 folding. The contradictions in the younging direction data near Vattuaho and N-S part of the Aho belt points to an isoclinal N-S folding which is a result from large scale thrusting systems or asymmetric folding.

Here I correlate the study area with the structural interpretation from the eastern and northern parts of Evijärvi bedrock map sheet 2314 (Vaarma, 1984, 1990). The study area is located at the western part of the bedrock map sheet and structural interpretation has not been done earlier from this area.

According to Vaarma (1984, 1990), four phases of deformation are present in the bedrock in Evijärvi. The first deformation feature is the bedding-parallel foliation S1 which is weak and rarely visible. This corresponds to the observations made in this study, as the bedding-parallel foliation can only be seen in thin sections. The stronger S2 foliation is

time to times of course parallel to the bedding at the limb zones of the folds. Vaarma noted that F1 folding is the reason for the variation of younging directions of stratigraphy for example in Pitkäsalo. The variation of younging directions is also present in the study area and this made it ambiguous to interpret the younging direction for example in the vicinity of N-S Aho metavolcanic belt near Vattuaho. The results of this study are in line with Vaarma's interpretation that the F1 folding is isoclinal and further highlight the character of overturning, which is attributed to the regional scale thrust systems.

The second deformational event in Vaarma's interpretation produced the penetrative foliation S2 which is the dominant foliation in almost every outcrop in the study area. According to Vaarma, mineral lineation parallel to the small-scale fold axes in quartz veins and the elongation of porphyroblasts and calc silicate concretions were produced during this second deformational event D2. Same applies to the study area.

In this study, this deformational event and foliation (S3) were interpreted to be younger than the NW-SE foliation present at the northern part of the study area (S2). Vaarma's D3 can be seen as crenulation cleavage S3 in pelite interlayers of supracrustal rocks. This foliation is rare outside the eastern and southern parts of Evijärvi, but it is debatable if the crenulation cleavage visible at the northern limb of the Mansikka-aho synform is equivalent to this S3 in Vaarma's interpretation (*Fig. 10a*; TJLE-2020-26). This crenulation cleavage is observed only in one outcrop and the crenulated older foliation is the local NE-SW trending axial plane foliation S2. According to Vaarma, this crenulation cleavage S3 have a dip direction towards south. The dip direction of crenulation cleavage in TJLE-2020-26 could not been measured, but the E-W strike corresponds to Vaarma's interpretation.

The fourth deformational event presented by Vaarma appears only locally at Kirsilä area which is located 5 to 10 kilometers east from the study area (*Fig. 1*). This folding with a style varying from open to tight deforms also the dominant S2 foliation, but signs of this foliation cannot be seen in the study area. The foliation generated after S3 in the study area is characterized by the posttectonic crystallization of muscovite.

The intrusions in the study area are younger than the supracrustal rock units. Age determination has been done to northern part of Aukeannevakangas intrusion and it is 1886 Ma +- 6 Ma (Vaasjoki et al., 1996). Vaarma noted that the intrusions cut the foliation of mica schist and the intrusions are not oriented enough to have gone through the

dominant D2 event. Vaarma concluded that the intrusions in the study area have been intruded after the D2 event. The results of this study do not contradict with the interpretation of Vaarma, because all the observations from the intrusions had no or only weak orientation.

In the tectonic evolution model by (Nironen et al., 2017) refined from several tectonic models made earlier (Lahtinen et al., 2005; Nironen, 1997), the D1 and the thrusting events with isoclinal folding in the study area corresponds to the accretion of Karelia and Norrbotten continental blocks. This event with SW-NE tectonic transport generated a metamorphic event which peaked at 1.91 Ga.

The main deformational features of D2 in the study area are equivalent with the collision of microcontinents Bergslagen and Keitele which resulted in the peak deformation and metamorphism during the early Svecofennian orogeny at 1.89-1.88 Ga (Lahtinen et al., 2005; Nironen et al., 2017). This produced compression with N-S orienting tectonic transport and N-S stress direction in the study area, which activated the NE-SW trending shear zones. The granodiorite and tonalite intrusions of the study area were intruded after this event and the older granitic veins are related to this magmatism (*table 1*).

Table 1. Summary of different deformation events compared to the visible structures, emplacement of dykes and veins and growth of metamorphic minerals in the study area.

Deformation event	Visible structures in Mansikka-aho	Emplacement of intrusions, dykes and veins	Growth of metamorphic minerals
D1 1.92 - 1.91 Ga Accretion of Karelia and Norrbotten continental blocks. (Nironen 1997, Lahtinen et al., 2005)	Isoclinal folding in the Mansikka-aho area. S1 foliation parallel to the primary bedding.	-	-
D2 1.89 - 1.88 Ga The collision of Bergslagen and Keitele microcontinents. (Lahtinen et al., 2005, Nironen et al., 2017)	F2 and the Mansikka-aho synform and antiform. The moderate to strong S2 foliation visible in almost every outcrop. Mineral lineation of quartz veins. Elongation of calc-silicate concretions and porphyroblasts.	Older, folded quartz veins. Post D2 tonalite, granodiorite and porphyritic granite intrusions. Granite dykes.	Pre-/earlytectonic sillimanite. Syntectonic sillimanite and K-feldspar. Posttectonic muscovite. Posttectonic andalusite.
D3 1.84 - 1.80 Ga Svecobaltic orogeny. (Lahtinen et al., 2005)	The crenulation cleavage S3.	Syn-D3 quartz veins. Post-D3 quartz veins. Post-D3 pegmatite and aplite dykes.	-

Based on the thin section study, the metamorphism in the study area occurred at medium pressure and high temperature conditions. The most typical metamorphic reaction occurred in the study area is a prograde dehydration reaction muscovite + quartz → K-feldspar + sillimanite + H20 (muscovite breakdown reaction). It is possible that a retrograde reaction K-feldspar + sillimanite + H20 → muscovite + quartz also happened if water was present at this stage, but another explanation for the occurrence of post-tectonic muscovite is the thermal effect from the emplacement of plutonic intrusions and the resulting contact metamorphism.

Fibrolitic sillimanite and K-feldspar blasts with internal foliation of biotite inclusions are typical for rocks with minerals crystallized in muscovite breakdown reaction (Carmichael, 1969). Sillimanite porphyroblasts do not display characteristic features of phase transition between andalusite and sillimanite, meaning that the muscovite

breakdown reaction occurred at the conditions where sillimanite was stable. It is possible that andalusite porphyroblasts crystallized later than sillimanite porphyroblasts, for example at the same time with muscovite porphyroblasts during the contact metamorphism.

Pajunen (2008) modelled the tectonic evolution in southern Finland during Svecofennian orogeny. This model contained clockwise rotation of crustal blocks, including Central Finland Granitoid Complex caused by dextral shear zones. This clockwise rotation is analogous to the situation and interpretation of structural and tectonic evolution of the study area (*Fig. 23*).

The two populations of quartz veins were placed during the late Svecofennian evolution which is characterized by crustal extension at the time period of 1.86 – 1.83 Ga (Nironen, 2005).

The pegmatites represent the youngest rock units in the study area and the intrusion of them relates to the post collisional magmatism at 1.80 – 1.76 Ga after a compressional event called Svecobaltic orogeny (Lahtinen et al., 2005).

5.5. Structural & lithological control of dykes and veins

Domain 1

Domain 1 hosts the largest number of dykes and veins. The quartz veins have at least two populations. The first population follows the E-W strike of the primary bedding and another population is parallel to the NW striking foliation. The pegmatites and aplites are systematically parallel to the foliation. This large number of veins is considered to reflect the presence of the interpreted shear zone. The position and orientation of the pegmatite dykes could imply dextral riedel-type veins, but the relative kinematics of the northern *shear zone 2* has been interpreted to be sinistral (*Figs. 21 & 23*).

The composition and rheology contrast of the supracrustal rocks seem to control the placement of the quartz veins. The psammite rich layers host more veins than the pelite layers, and the psammite hosted veins are usually wider. This cannot be seen in the more limited pegmatite and aplite dataset.

The relative widths of the veins and dykes can be used as indicators of the stress field during the vein placement (Jolly & Sanderson, 1997). The larger width means larger opening and the opening direction corresponds to the minimum principal stress component (sigma 3). Both domains 1 and 2 are characterized by wider dykes and veins in the E-W direction corresponding to the N-S direction of sigma 3 at the time of emplacement.

Based on the relationships of the two main vein populations, the E-W veins (with larger space opening for the vein material) are younger than the thinner N-S vein population. When comparing the age relationships between the different types of the dykes and veins, the repeating trend observed at the outcrops is that the pegmatites are younger than the quartz veins. The dykes documented as granite dykes intruded at an earlier stage than the pegmatites, aplites and quartz veins.

Domain 2

The dykes and veins in domain 2 typically follow the orientation of the NE foliation. This foliation is the axial plane foliation of the Mansikka-aho synform.

Domain 2 has the same pattern with vein and dyke width and age relationships than domain 1. The differing orientations of the older quartz vein populations in domains 1 and 2 are due to the opening of the foliation planes. These differing orientations are not always the result of the different and diverging stress fields. Differently oriented structures can be generated in a same stress field when the reference plane of the studied structure has a different orientation. For example, when comparing the dykes relative to the northern E-W limb of the Mansikka-aho synform to the NE-SW southern limb, the space released for the veins happens in a different direction and diverging veins are formed. This can happen when the stress field is the same.

One stress field with N-S sigma 3 could explain the opening of both the foliation planes in domain 1 and 2, resulting in the first foliation-parallel population of quartz veins. As the E-W planes, such as primary bedding planes in domain 1, activated in this stress field at a later stage, these structures got more space to open and wider veins to form.

Domains 3 and 4

The dykes and veins in the intrusions occur mainly at the contact zones of the intrusive and supracrustal rocks. The occurrence of the dykes is not relative to the uneven abundance of the outcrops, because the central areas of the intrusions do also have bedrock outcrops. The Nauriskallio quarries are an example of this uneven distribution of the dykes. The two construction aggregate quarries close to the contact zone host numerous pegmatite veins. The other quarry is located closer to the center of the intrusion, but it lacks pegmatites and quartz veins. These dykes and veins have two populations, parallel and perpendicular to the contact.

The dykes and veins do not show similar patterns with vein width and the orientation relative to the stress field than the domains 1 and 2. The N-S striking pegmatite and granite dykes tend to be wider than E-W striking.

The two populations of dykes, parallel and perpendicular to the intrusion, might have intruded the space generated by cooling and contraction of the intrusions. In the analogue modelling by Ellis & Blenkinsop (2019), two fracture sets were generated during the cooling and contraction. One set was generated perpendicular to the intrusion contact with subvertical dips and another set was characterized by concentric fractures that curved downwards as the depth increased. In this modelling, most of the fractures were produced at the margins of the intrusions and the number of fractures decreased towards the center of the intrusion. In this analogue modelling the number of fractures decreased when the sample material was buried deeper. As a conclusion, the younger pegmatite dykes in the intrusions of the study area have utilized the pathways formed by the cooling and contraction of the intrusions.

The presented structural interpretation of the study area is plausible when studying the northern continuities of the Aho metavolcanic belt where GTK has a valid exploration permit, and where the exploration areas of Keliber are located. The shear zone bounded blocks with z-symmetrical folding visible in the aeromagnetic map at the Kaustinen area makes it a similar structural framework with the study area and the southern part of the metavolcanic belt (*Fig. 22*). Further study subjects concerning the mineral potential of the pegmatites within the study area could be the fertility studies of the pegmatite granites approximately 5 – 15 kilometer south from the study area.

6. Conclusions

- The study area is characterized by a plunging synform and an overturned plunging antiform with fold axes pointing towards SW.
- This structure is enclosed within a larger open fold within the Ostrobothnia schist belt.
- The stratigraphy of the study area is largely over-turned from its original depositional position.
- The geometry of the study area is controlled by NE-trending shear zones located north and south of the study area. The study area represents a shear-bound block which got its final geometry because of a transpressional clockwise rotation between shear zones. The overall movement at this event was dextral.
- At least three major deformation events have occurred within the study area:
    1. D1 which is related to regional-scale thrusting systems and isoclinal folding. Overturned features and inverted stratigraphy in the study area is probably a result of this deformation event. The structures related to this event are weak in the study area and they are typically only visible in thin sections as a foliation parallel to the primary bedding.
    2. D2 which represents the peak of the deformation and the most dominant structural features in the outcrops of the study area.
    3. D3, which can be seen as crenulation cleavage S3 in individual outcrops at the northern part of the study area
- The bedrock of the study area is mainly composed of mica schists, black schists, metavolcanic rocks, felsic intrusions, quartz veins and pegmatite and aplite dykes.
- The age relationship of the veins and dykes at the study area is:
    1. Folded, D2 quartz veins.
    2. Post-D2 granitic dykes related to the tonalite and granodiorite intrusions.
    3. Syn-D3 quartz veins.
    4. Post-D3 quartz veins.
    5. Post-D3 pegmatite dykes.
- Pegmatite dykes and quartz veins in the tonalite and granodiorite intrusions are concentrated at the margins of intrusions. The veins and dykes occur both parallel

to the contact and perpendicular to the contact. The number of veins and dykes decreases towards the center of the intrusions. The orientation and spatial distribution of the dykes and veins at the intrusions are related to the local stress field, rather than the regional stress field. This local stress field is generated by the intrusion, the cooling, and the contraction of the intrusions.

- The intrusion of the pegmatite veins and the quartz veins in the supracrustal rocks are controlled by the structures of the bedrock, but also by the lithology and the rheology contrast. The veins and dykes are emplaced at the older planar structures such as the foliation and the bedding planes. The psammite interlayers in supracrustal rocks host most of the quartz veins while they are less common in pelitic layers.
- The later quartz veins are divided in two main populations. The older population (syn-D3) preferred the NW-SE and NE-SW trending structures such as the foliation planes and the younger population (post-D3) preferred the structures which are trending closer to the E-W direction such as the primary bedding planes.
- The Nauriskallio tonalite and the Hautamaa porphyritic granodiorite are two separate plutonic units.

7. Acknowledgements

To begin with, I would like to thank professor Pietari Skyttä for his guidance throughout my thesis and during my studies in the University of Turku. Professor Skyttä's expertise in field and in structural geology made this work possible.

I would like to thank MSc Janne Kuusela for selection of the subject and study area for this thesis, and for the opportunity to work with him and the Geological Survey of Finland during the field seasons of 2019 and 2020.

I would like to express my gratitude to geologists Alexandra Jónsdóttir and Henrik Nygård for our memorable teamwork during my internship at the Geological Survey of Finland and for their assistance in bedrock mapping and handheld rock drilling in Mansikka-aho.

I would like to thank laboratory technician Arto Peltola for the preparation of thin sections and for the help and guidance related to thin section study.

Additionally, I would like to thank PhD Markku Väisänen for discussion related to the thin section study, PhD Jussi Mattila for guidance related to paleostress analysis and stress field modelling, professor Esa Heilimo for guidance in GIS-related problems and PhD Timo Kilpeläinen for work related to revision of this thesis.

Finally, I would like to thank Geohouse personnel and my student colleagues for our shared time in Turku.

8. References

Ahtola, T., Kuusela, J., Käpyaho, A. & Kontoniemi, O. 2015. Overview of lithium pegmatite exploration in the Kaustinen area in 2003–2012. *Geological Survey of Finland*. pp. 363–387.

Ahtola, T., Kuusela, J., Koistinen, E., Seppänen, H., Hatakka, T. & Lohva, J. 2010. Report of investigations on the Syväjärvi lithium pegmatite deposit in Kaustinen , Western Finland. *Geological Survey of Finland.* 33p.

Blengini, G. A., Latunussa, C., Eynard, U., Torres de Matos, C., Wittmer, D., Georgitzikis, K., Pavel, C., Carrara, S., Mancini, L., Unguru, M., Blagoeva, D., Mathieux, F. & Pennington, D. 2020. Study on the review of the list of Critical Raw Materials - Final Report. *Critical Raw Materials Factsheets*. 153p.

Carmichael, D. M. 1969. On the Mechanism of Prograde Metamorphic Reactions in Quartz-Bearing Pelitic Rocks. *Contributions to Mineralogy and Petrology*, 20, pp. 244-267.

Deveaud, S., Gumiaux, C., Gloaguen, E. & Branquet, Y. 2013. Spatial statistical analysis applied to rare-element LCT-type pegmatite felds: An original approach to constrain faults-pegmatites-granites relationships. *Journal of Geosciences (Czech Republic)*, *58*(2). pp. 163–182.

Dill, H. G. 2015. Pegmatites and aplites: Their genetic and applied ore geology. *Ore Geology Reviews*, *69*. pp. 417–561.

Ellis, J. F. & Blenkinsop, T. 2019. Analogue modelling of fracturing in cooling plutonic bodies. *Tectonophysics*, *766*(May). pp. 14–19 .

Geological Survey of Finland. 22.6.2021. *Hakku-palvelu*. https://hakku.gtk.fi/.

Hulsbosch, N., Van Daele, J., Reinders, N., Dewaele, S., Jacques, D. & Muchez, P. 2017. Structural control on the emplacement of contemporaneous Sn-Ta-Nb mineralized LCT pegmatites and Sn bearing quartz veins: Insights from the Musha and Ntunga deposits of the Karagwe-Ankole Belt, Rwanda. *Journal of African Earth Sciences*, *134*. pp. 24–32.

Jolly, R. J. H. & Sanderson, D. J. 1997. A Mohr circle construction for the opening of a pre-existing fracture. *Journal of Structural Geology*, *19*(6). pp. 887–892.

Kuusela, J., Ahtola, T., Koistinen, E., Seppänen, H., Hatakka, T. & Lohva, J. 2011. Report of investigations on the Rapasaaret lithium pegmatite deposit in Kaustinen-Kokkola, Western Finland. *Geological Survey of Finland.* 40p.

Kuusela, J. & Kaunismäki, J. 2020. Investigations of the Kellokallio spodumene pegmatite in Veteli , Western Finland. *Geological Survey of Finland.* 12p.

Lahtinen, R., Korja, A. & Nironen, M. 2005. Paleoproterozoic tectonic evolution. *Precambrian Geology of Finland - Key to the Evolution of the Fennoscandian Shield*. pp. 481–532.

Marmo, V. 1960. On the sulphide and sulphide-graphite schists of Finland with an especial reference to the sulphide-graphite schists of Central Pohjanmaa. *Geological Survey of Finland*. 86 p.

National Land Survey of Finland. 22.6.2021. Avoimien aineistojen tiedostopalvelu. https://tiedostopalvelu.maanmittauslaitos.fi/tp/kartta.

Nironen, M. 2005. Proterozoic orogenic granitoid rocks. *Precambrian Geology of Finland - Key to the Evolution of the Fennoscandian Shield*. pp. 99-117.

Nironen, M. 1997. The Svecofennian Orogen: a tectonic model. In *Precambrian Research (Vol. 86)*. pp. 21-44.

Nironen, M., Luukas, J., Kousa, J., Vuollo, J., Holtta, P. & Heilimo, E. 2017. Bedrock of Finland at the scale 1:1 000 000 – Major stratigraphic units, metamorphism and tectonic evolution. *Geological Survey of Finland, Special Paper (Vol. 60)*. 128p.

Partington, G. A. 1990. Environment and Structural Controls on the Intrusion of the Giant Rare Metal Greenbushes Pegmatite, Western Australia. *Economic Geology*, *85*. pp. 437–456.

Rasilainen, K., Eilu, P., Ahtola, T., Halkoaho, T., Kärkkäinen, N., Kuusela, J., Lintinen, P. & Törmänen, T. 2018. Quantitative assessment of undiscovered resources in lithium-caesium-tantalum pegmatite-hosted deposits in Finland. *Bulletin of the Geological Survey of Finland (Vol. 406)*. 172p.

Ruskeeniemi, K. 1988. Mustaliuskeiden metallipitoisuuksista Kaustisen ja Evijärven karttalehtien alueella. 10p.

Sales, E. D. G., Genuíno, V. A., Santos, L. C. M. de L., Vieira, F. F. & Vidal, F. W. H. 2016. The Role of Brittle Structures on the Emplacement of Mineralized Pegmatites in the Pedra Lavrada Disctrict, NE Brazil. pp. 90–97.

Simonen, A. 1980. The Precambrian in Finland. *Geological Survey of Finland, Bulletin*, *304*. 58p.

Vaarma, M. 1984. Pohjanmaan liuskevyöhykkeen geologia Evijärven alueella. *Pro gradu -tutkielma, Helsingin yliopisto, geologian laitos.* 143p.

Vaarma, M. 1990. Pohjanmaan liuskevyöhykkeen geologia Evijärven alueella. *Lisensiaattitutkielma, Helsingin yliopisto, geologian laitos.* 100p.

Vaarma, M. & Kähkönen, Y. 1994. Geochemistry of the Paleoproterozoic metavolcanic rocks at Evijärvi, Western Finland. *Geological Survey of Finland, Special Paper 19*. pp. 47-59.

Vaarma, M. & Pipping, F. 1997. Alajärven ja Evijärven kartta-alueiden kallioperä. *Geological Survey of Finland*. 83p.

Vaasjoki, M., Pietikäinen, K. & Vaarma, M. 1996. U-Pb zircon determinations from the Keikyä breccia and other sites in the Svecofennides: indications of a Svecokarelian protocrust. *Bulletin of the Geological Society of Finland*. pp. 3-10.

Veriö, A., Kuivamäki, A. & Vuorela, P. 1993. Kallioperän murroslinjojen nykyliikunnoista - Maanmittauslaitoksen murroslinjavaaitukset 1974-1992 osa II. *Geological Survey of Finland*. 50p.

Vuorela, P. 1982. Crustal fractures indicated by lineament density, Finland. *Geological Survey of Finland*. 16p.

Appendix 1: All dyke and vein observations in the study area

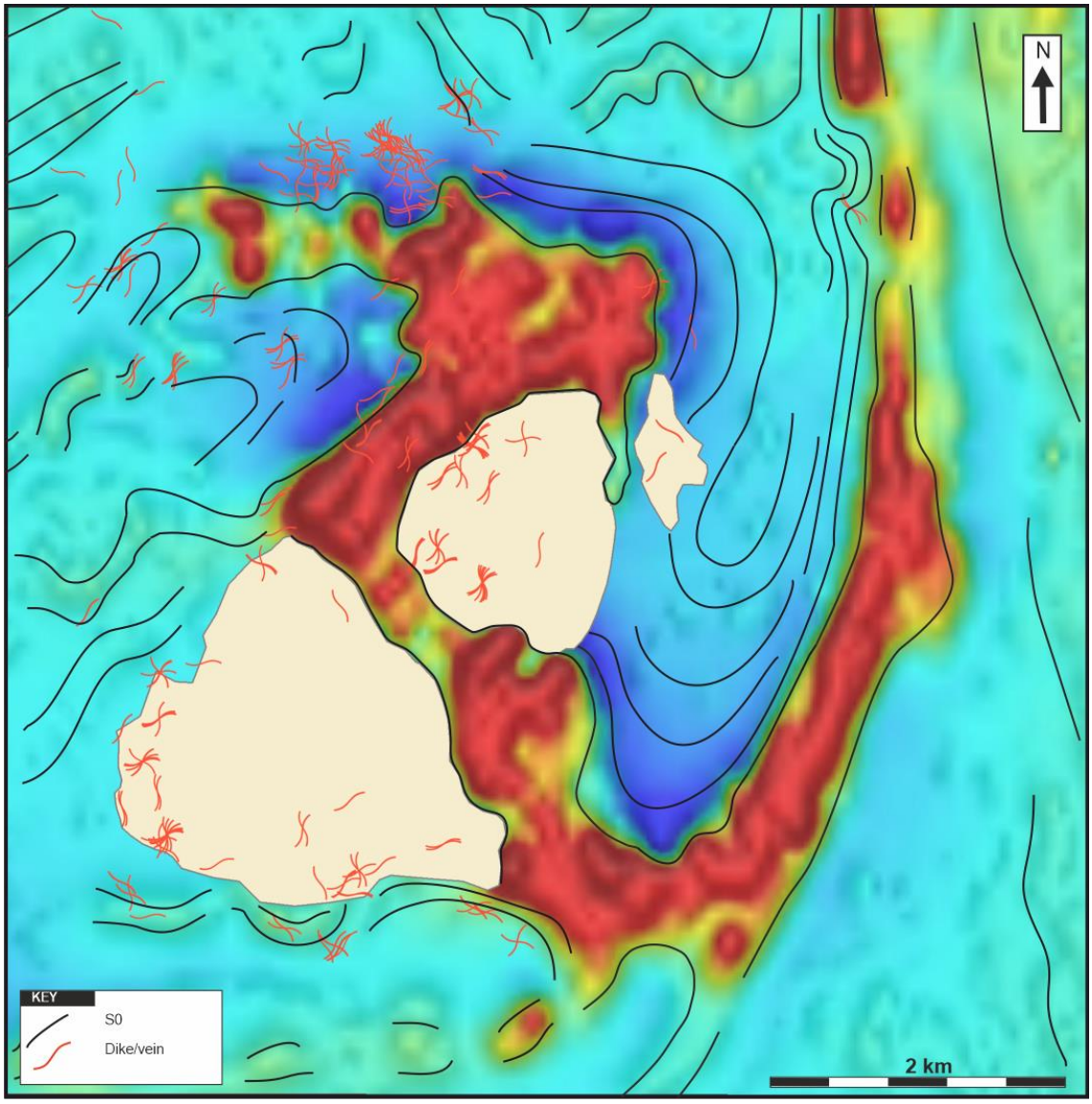

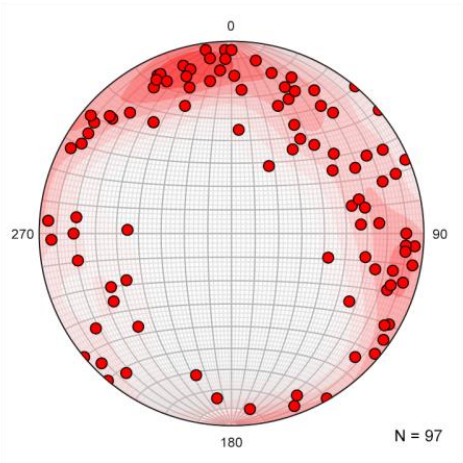

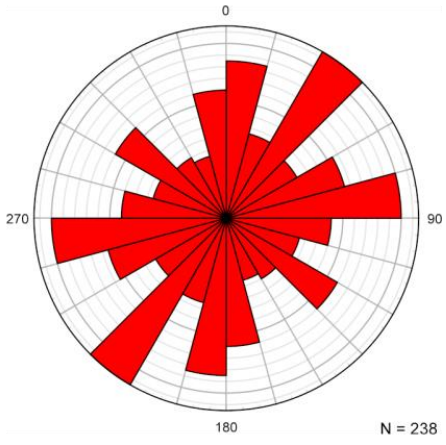

Appendix 2: Foliation observations

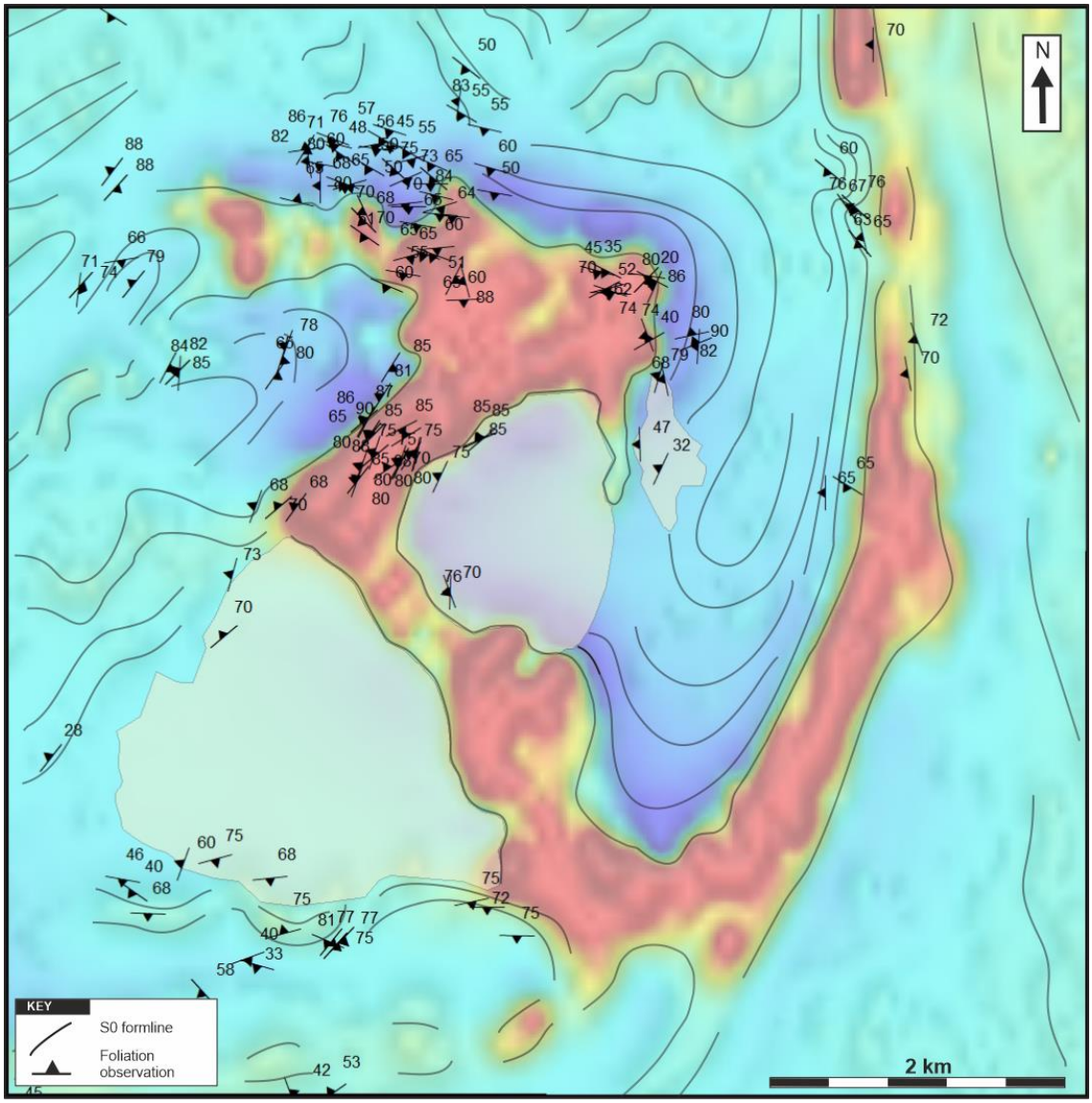

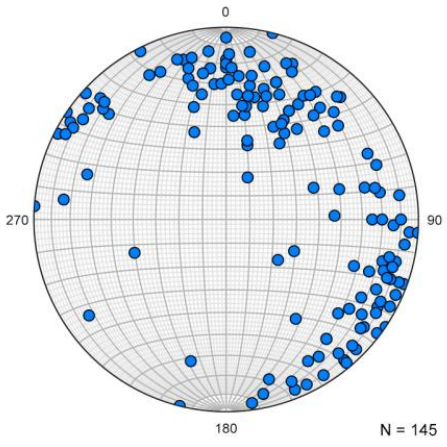

Appendix 3: Bedding observations

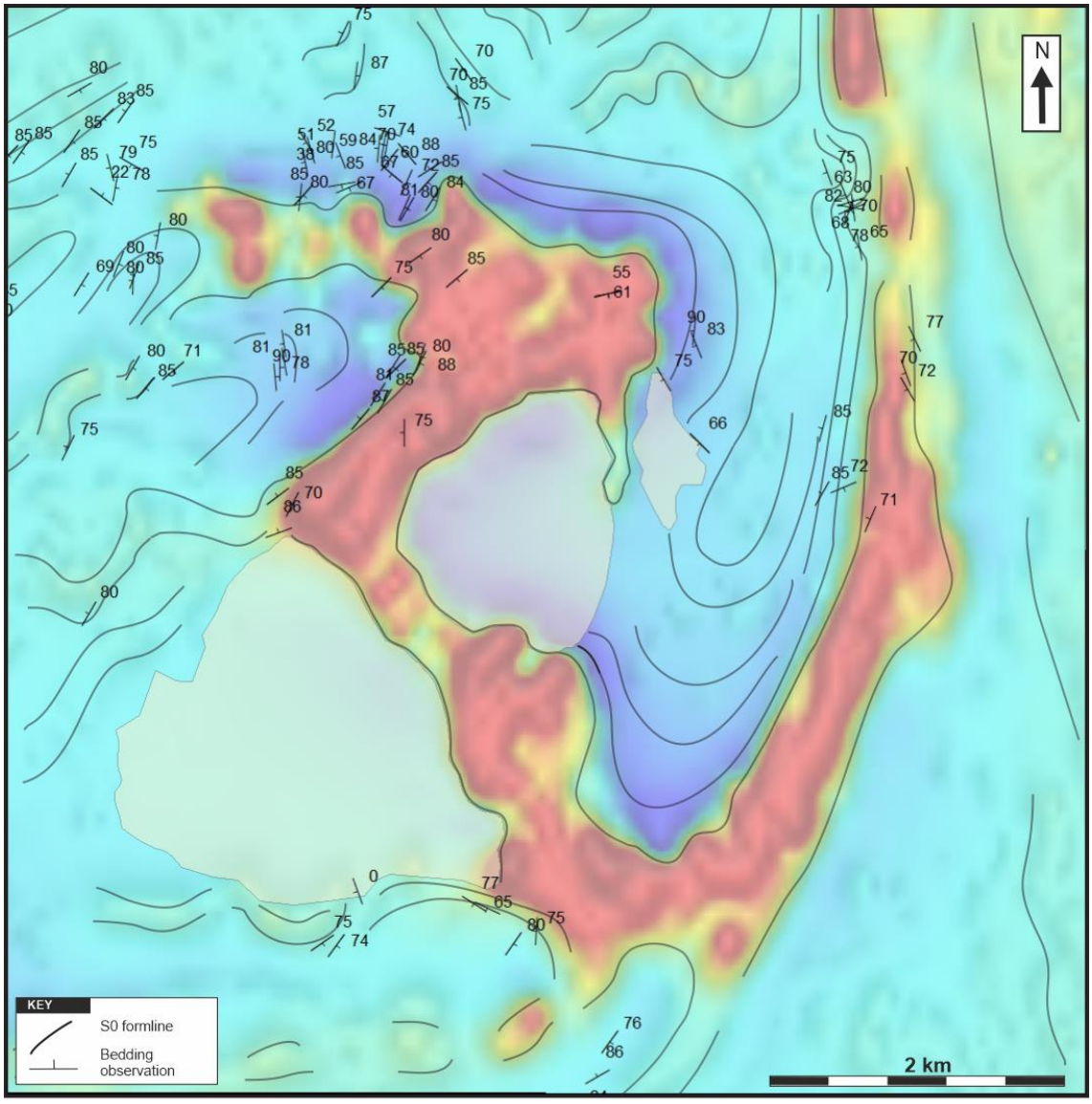

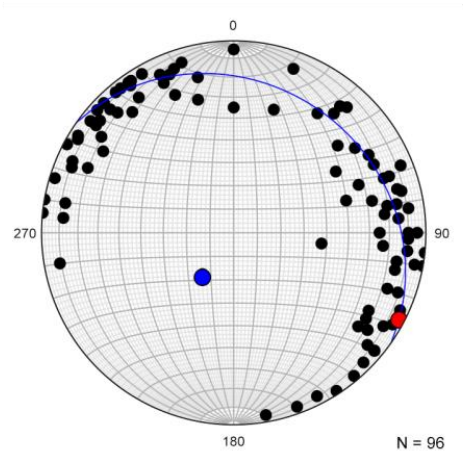

Appendix 4: Coordinates of the observations

Observation id	X	Y	Observation id	X	Y	Observation id	X	Y	Observation id	X	Y
TJLE-2019-78	320444,9051	7031702,457	**TJLE-2020-1**	319130,796	7032675,477	**TJLE-2020-28**	318574,2251	7032683,463	**TJLE-2020-56**	319092,1462	7032455,147
TJLE-2019-79	320484,4927	7031697,218	**TJLE-2020-2**	318228,4884	7031353,96	**TJLE-2020-29**	318609,4892	7032631,149	**TJLE-2020-57**	319076,6315	7032284,089
TJLE-2019-83	319103,1278	7031944,078	**TJLE-2020-3**	317006,5481	7032374,644	**TJLE-2020-30**	318607,5113	7032524,649	**TJLE-2020-58**	317446,4872	7063759,544
TJLE-2019-84	319085,8928	7031947,317	**TJLE-2020-4**	319374,5314	7031838,536	**TJLE-2020-31**	318692,2273	7032407,338	**TJLE-2020-59**	319101,4519	7067761,141
TJLE-2019-85	319074,8628	7031908,534	**TJLE-2020-5**	319431,5904	7031789,008	**TJLE-2020-32**	318909,0217	7032725,026	**TJLE-2020-60**	315786,9602	7072115,303
TJLE-2019-87	319326,6779	7031902,663	**TJLE-2020-6**	319282,2354	7029977,151	**TJLE-2020-33**	319231,0858	7032566,238	**TJLE-2020-60**	315786,9602	7072115,303
TJLE-2019-88	319367,5212	7031832,806	**TJLE-2020-7**	320801,9262	7031113,092	**TJLE-2020-34**	319109,1603	7032581,066	**TJLE-2020-61**	325871,0158	7057195,223
TJLE-2019-89	319409,7345	7031761,662	**TJLE-2020-8**	320720,5871	7031789,332	**TJLE-2020-35**	317123,7296	7032413,122	**TJLE-2020-62**	322351,6952	7055834,262
TJLE-2019-90	318835,6289	7030619,872	**TJLE-2020-9**	320728,9585	7031768,8	**TJLE-2020-36**	317049,0558	7032556,411	**TJLE-2020-62**	322351,6952	7055834,262
TJLE-2019-91	319000,4264	7030569,665	**TJLE-2020-10**	320736,0153	7031763,937	**TJLE-2020-37**	319981,4589	7051490,363	**TJLE-2020-63**	317197,6098	7031790,336
TJLE-2019-92	320699,5584	7031389,159	**TJLE-2020-11**	320442,7614	7031707,593	**TJLE-2020-38**	316883,9557	7031752,988	**TJLE-2020-64**	317136,5323	7031898,626
TJLE-2019-93	320724,8054	7031346,884	**TJLE-2020-12**	320454,4669	7031676,065	**TJLE-2020-39**	316872,6045	7031734,257	**TJLE-2020-65**	317418,0103	7029143,241
TJLE-2019-94	320764,7962	7031351,616	**TJLE-2020-13**	322105,5715	7032276,896	**TJLE-2020-40**	319341,9129	7029677,928	**TJLE-2020-66**	318265,6785	7031238,202
TJLE-2019-95	320779,1186	7031329,151	**TJLE-2020-14**	322106,366	7032256,368	**TJLE-2020-41**	318586,2066	7027266,844	**TJLE-2020-67**	318271,629	7031150,173
TJLE-2019-98	320831,9629	7031625,521	**TJLE-2020-15**	322100,9356	7032304,084	**TJLE-2020-42**	318617,886	7027254,009	**TJLE-2020-68**	324493,1422	7063603,765
TJLE-2019-99	320667,6249	7031894,126	**TJLE-2020-16**	319441,6961	7030494,01	**TJLE-2020-43**	318656,0107	7027276,136	**TJLE-2020-69**	320756,566	7031158,588
TJLE-2019-100	318301,7914	7030259,693	**TJLE-2020-17**	319557,5819	7030735,686	**TJLE-2020-45**	317487,0787	7031196,23	**TJLE-2020-70**	320706,2215	7031412,119
TJLE-2019-101	318283,9791	7030030,302	**TJLE-2020-18**	319004,6156	7030559,107	**TJLE-2020-46**	318947,7441	7032777,508	**TJLE-2020-71**	321015,9439	7031450,826
TJLE-2019-102	318726,3118	7030457,057	**TJLE-2020-19**	319108,6161	7030617,733	**TJLE-2020-47**	319392,5637	7033010,694	**TJLE-2020-72**	321030,6641	7031391,588
TJLE-2019-103	320174,7596	7030691,582	**TJLE-2020-20**	319054,7777	7030753,865	**TJLE-2020-48**	319417,7151	7033044,699	**TJLE-2020-73**	321032,2594	7031343,345
TJLE-2019-104	320872,0636	7030705,08	**TJLE-2020-21**	319003,7126	7031188,456	**TJLE-2020-49**	319823,5194	7027299,376	**TJLE-2020-74**	319323,9988	7032259,62
TJLE-2019-105	321925,581	7030799,824	**TJLE-2020-22**	318874,7614	7031019,249	**TJLE-2020-50**	318145,2904	7027704,884	**TJLE-2020-75**	319266,2556	7032330,376
TJLE-2019-110	318772,7953	7030850,38	**TJLE-2020-23**	318769,7501	7030847,206	**TJLE-2020-51**	318876,6914	7032658,116	**TJLE-2020-76**	319242,3111	7032419,011
TJLE-2019-111	318798,6465	7030754,891	**TJLE-2020-24**	318806,639	7030761,139	**TJLE-2020-52**	318873,2105	7032689,345	**TJLE-2020-77**	319300,906	7029853,027
TJLE-2019-112	319112,7134	7030629,045	**TJLE-2020-25**	318565,0738	7032725,35	**TJLE-2020-53**	318968,9108	7032688,302	**TJLE-2020-78**	318382,0114	7032608,93
TJLE-2019-113	319562,3296	7030744,851	**TJLE-2020-26**	318413,8971	7032675,06	**TJLE-2020-54**	318966,3693	7032612,374	**TJLE-2020-79**	318461,5897	7032441,665
TJLE-2019-114	319574,1509	7030728,412	**TJLE-2020-27**	318389,1559	7032720,425	**TJLE-2020-55**	318984,4945	7032520,66	**TJLE-2020-80**	318396,0789	7032372,478
									TJLE-2020-81	318330,8149	7032370,554